Chapter 8
Directed Assembly and Self-organization of Metal Nanoparticles in Two and Three Dimensions

S. Holger Eichhorn and Jonathan K. Yu

Abstract Properties of metals and other compounds change in comparison to their bulk materials when they are prepared as sufficiently small particles, usually in the 1–50 nm range. A myriad of applications for these nanoparticles have been conceived and tested and their presence in consumer products is already ubiquitous. It was established right from the beginning that the properties of materials containing nanoparticles not only depend on their size, shape, and composition but also their spatial arrangement. Most prominent are predictable changes to their optical properties when nanoparticles are positioned in ordered arrays and sufficiently close to permit electronic interactions. This chapter describes the recent advancements in the arrangement of metal nanoparticles into defined structures of two- and three-dimensional order by the Langmuir-Blodgett technique, layer-by-layer deposition, and the self-organization of liquid crystalline and amphiphilic metal nanoparticles. The large volume of work on the (directed) self-assembly of nanoparticles is just briefly presented in the introduction as it has been extensively and comprehensively reviewed by others. While the Langmuir-Blodgett technique can generate monolayer and multilayer materials, the other two techniques (layer-by-layer deposition and the self-organization) are predominantly applied to the preparation of three-dimensionally ordered materials. Discussed in great detail is how the purity and size-distribution of employed metal nanoparticles and the structure of their protective layer(s) affect their ability to generate two- and three-dimensionally ordered arrangements of high quality and persistence length by any of the three techniques. Processing conditions are described in less detail because they do not differ from those used for molecular materials, although they are equally important to the preparation of structures of long-range order. Finally, possible applications and properties of materials prepared by the Langmuir-Blodgett technique, Layer-by-layer deposition, and self-organization are described if deemed important.

S. Holger Eichhorn (✉) · J.K. Yu
Department of Chemistry and Biochemistry, University of Windsor,
401 Sunset Avenue, Windsor, ON N9B 3P4, Canada
e-mail: eichhorn@uwindsor.ca

Q. Li (ed.), *Anisotropic Nanomaterials*, NanoScience and Technology,
DOI 10.1007/978-3-319-18293-3_8

8.1 Introduction

Both, molecular and supramolecular structures affect the properties of molecular materials and must be optimized for every desired application. Similarly, properties of materials comprised of metal nanoparticles (MNPs) are controlled not only by the structure and composition of MNPs but also their arrangement in space. In fact, an increasing proportion of the recent research on MNPs has focused on their controlled processing into specific one-, two-, and three-dimensional structures. Self-assembly and self-assembly directed or assisted by directional chemical interactions, external fields, and template surfaces, are the most prominent methodologies applied to control the spatial arrangement of nanoparticles (NPs) but structures of two- and three-dimensional order have also been obtained with other techniques, such as the formation of Langmuir-Blodgett (LB) films, Layer-by-Layer (LbL) deposition, and the self-organization of liquid crystalline or amphiphilic MNPs (Fig. 8.1). It is the application of the latter three techniques this chapter is concerned with, in addition to being focused on MNPs, since the application of self-assembly and related processes has been recently and extensively reviewed by others [1–5]. Brief summaries of selected review articles on the controlled assembly

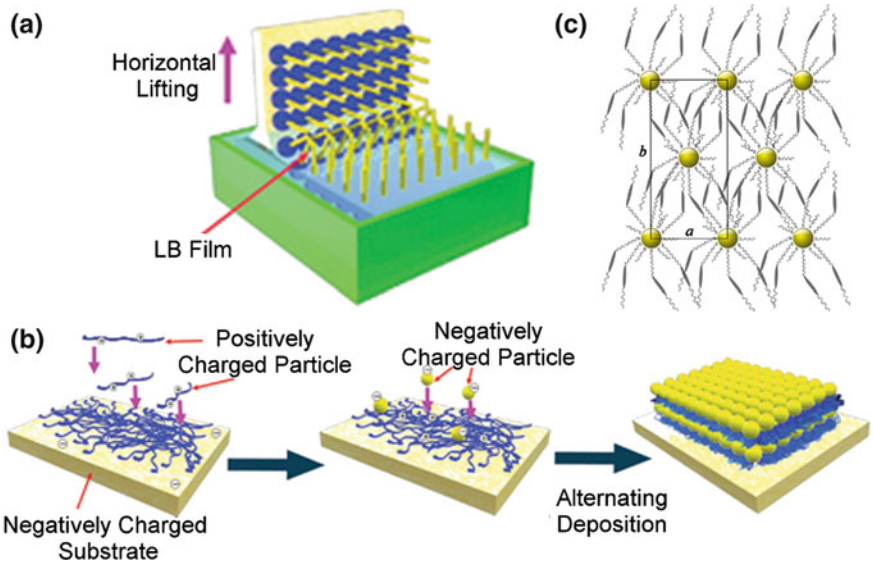

Fig. 8.1 Cartoons of ordered structures generated by **a** LB films, **b** LbL deposition [6], and **c** the self-organization of liquid crystalline or amphiphilic MNPs [7]. Adapted by permission from Macmillan Publishers Ltd.: NPG Asia Materials [6], copyright 2012. Reprinted (adapted) with permission from [7]. Copyright 2013 American Chemical Society

of nanoparticles by techniques not covered here are provided below as guidance for the interested reader.

Grzelczak et al. review mainly the directed self-assembly of spherical gold NPs and, in more general terms, to what extent self-assembly can be controlled by either changing the energy or entropy landscapes via the use of templates or applied external fields [1]. The first part is concerned with the interactions between chemically modified gold NPs and templates and the template free self-assembly of chemically modified gold NPs due to directional interactions. Provided examples include DNA mediated assembly of gold NPs and investigations of anisotropic and Janus-type MNPs. The second part briefly describes the influence of various external fields on the self-assembly process, which inevitably includes examples of metal oxide, modified polymer, silica, and other NPs. Besides the common application of a single field (electric, magnetic, and flow), the authors also highlight the high potential for simultaneous application of several directing fields. This second part also includes a short overview of self-assembly of NPs at liquid-liquid interfaces but the interested reader may rather be directed to a comprehensive review on self-assembly at liquid-liquid interfaces by Böker et al. [2].

Although already 7 years old, the review on self-assembly of NPs by Kinge et al. is still one of the most comprehensive description of different self-assembly processes and their principles [3]. At the centre of this review is the description of different self-assembly methods and their underlying principles, such as drying mediated assembly, self-assembled monolayers, self-assembly via H-bonding, electrostatic assembly including LbL deposition, directed assembly aided by electrical, magnetic, and optical fields, and assembly at interfaces that includes a short section on LB films. Also described is the use of inorganic and biological templates, microcontact and other printing methods, as well as shape-selective assembly of non-spherical NPs. Following the part on general concepts and methodology is an extensive list of examples that is structured based on the dimensionality (one, two, and three) of the self-assembly and the review concludes with a brief description of specific properties of self-assembled NPs. A more concise and recent account on techniques for self-assembly of NPs is provided by Nie et al., which also gives a more comprehensive description of the properties of derived materials and their potential applications [4]. The authors in particular emphasize properties that derive from plasmonic interactions and the same research group has recently devoted an entire review to the subject of self-assembled plasmonic nanostructures [5]. This review, in contrast to all other reviews mentioned here, also contains a part on the computational modelling of self-organization of NPs and discusses the dynamic and static nature of NP assemblies. A quotation from this review will serve us as a final remark: “We note that although a particular force may dominate the self-assembly process, in reality, the formation of a particular structure originates from the interplay of several forces.”

8.2 Langmuir-Blodgett Films of Metal Nanoparticles (MNPs)

8.2.1 Introduction

The Langmuir-Blodgett (LB) technique is probably the oldest methodology for the generation of defined monomolecular layers and their layer-by-layer transfer onto substrates. So, it is not surprising that NPs were processed into monolayers by the LB technique as soon as they became available as soluble, discrete, and well characterized entities. In the early 1990s Peng and co-workers already described the formation of LB films of Fe_2O_3 NPs with stearate layers in between the NP layers [8]. Since then, the LB technique has been applied to many other types of NPs, such as NPs made of metal [9] and metal oxides [10], NPs with core-shell structures [11], and NPs that are semiconductors [12] or magnetic [13]. This review is mainly concerned with metal NPs (MNPs) but NPs generated from metal oxides and inorganic semiconductors may be mentioned where appropriate. Not covered is the synthesis of MNPs used for LB deposition although specific purity or shape requirements may be indicated.

When compared to other assembling methods, such as self-assembled monolayer templates and lithographic patterning, the LB method has several important advantages: (a) relatively large areas can be uniformly coated (square centimeters) for comparatively low cost, (b) the spacing between MNPs can be relatively easily varied by adjusting the surface pressure, (c) basically all soluble MNPs can be processed by this method, (d) monolayers of two-dimensional order and multilayers of three-dimensional order can be generated [14]. Important deficiencies of the LB method are limited scalability and the incompatibility with continuous coating processes.

In general, the formation of LB films of MNPs involves the following four steps: (1) The MNPs must be dissolved in a sufficiently volatile solvent that is immiscible with the mostly aqueous subphase of the trough. (2) This solution is spread onto the water surface to generate a Langmuir film after the evaporation of the solvent. (3) The physical state of the Langmuir film is controlled and changed with moveable barriers that adjust the available surface area and, consequently, surface pressure. (4) The Langmuir film is transferred, usually by vertical dipping (Langmuir-Blodgett technique) or horizontal lifting (Langmuir-Schäfer technique), onto a substrate at a surface pressure below the collapse pressure of the film to generate a LB film [15, 16].

All MNPs used for depositions by the LB method are coated with a monolayer or bilayer layer of organic protecting ligands or with a polymer layer to prevent particle growth by coalescence [17] and to impart sufficiently high solubility in the spreading solvent and perhaps an amphiphilic character. A stable and adequate spacing between metal cores of MNPs is particularly important when the film is compressed to avoid coalescence, which usually results in a loss of the assembled structure due to precipitation [18, 19]. Compression to surface pressures of 10 mN/m and larger is essential for the generation of uniform films of close-packed

MNPs. L-films with collapse pressures much larger than 15 mN/m usually require sufficiently amphiphilic MNPs, which is not easily achieved [20]. Two common approaches to amphiphilic MNPs is the preparation of Janus MNPs, nanoparticles that possess two different chemical functionalities at each hemisphere, such as one hydrophobic and one hydrophilic side [21], or the coating with amphiphilic polymers [22]. Alternatively, less amphiphilic MNPs have been co-deposited with an amphiphilic reagent (surfactant), which certainly is the most straightforward approach and avoids complex synthetic pathways [23]. Clearly, many properties of the MNPs important to the formation of L- and LB-films are controlled by their protective coating, which is why we structured the following part of individual contributions based on the types of coatings, with the exception of the part on magnetic MNPs.

Before we begin with the discussion of individual papers we should provide some general information on the processing of MNPs by the LB method and guidance on how to interpret published results. We start with typical conditions for the processing of L-films and LB-films. Most common spreading solvents are chloroform and toluene but limited solubility especially of charged MNPs required the use of solvent mixtures such as dimethyl sulfoxide (DMSO) and chloroform. Concentrations of the MNPs in the spreading solvent are rarely provided because their low solubility usually requires 1–5 mL of saturated solution. These large volumes must be carefully and dropwise added at different locations of the liquid subphase to avoid early formation of three-dimensional aggregates. MNPs much larger than 20 nm in diameter are usually not sufficiently soluble and are spread as dispersions after extensive sonication. The most common subphase still is ultrapure water but especially hydrophobic MNPs have been reported to spread better on ethylene glycol and diethylene glycol [24].

A common problem with MNPs is their strong propensity for self-aggregation into islands of solid domains or even three-dimensional aggregates. This may be circumvented by a careful spreading procedure and fast enough compression of the L-film. Typical reported compression rates are between 5 and 15 cm^2/min and maximum surface pressures before buckling of the L-film occurs are 10–15 mN/m. However, much higher collapse pressures of 30 mN/m and larger have also been reported. Defects in the rigid monolayers may be improved by compression-expansion cycles if the compression is at least partially reversible [25]. Both, the collapse pressure and the packing order of MNPs in the L-film critically depend on the purity of the MNPs and their size distribution, which complicates the comparison of results obtained by different groups. Especially the presence of excess protective ligand or polymer is often not carefully evaluated and may be the main reason for a less ordered packing. We also note that the evaluation of the phase behaviour in L-films solely based on pressure-area isotherms can be rather misleading. Studies of the phase behaviour must be accompanied at least by Brewster angle microscopy while the analysis of transferred LB films may not provide reliable information on the structure of the preceding L-film, especially if transferred at low surface pressures.

Transfer of L-films onto hydrophilic and hydrophobic substrates is usually achieved by vertical up-stroke (LB-technique) or horizontal lift-up (Langmuir-Schäfer technique) at speeds of 0.1–1.0 mm/min. In some studies the up-stroke angle was altered to values of around 105° to minimize film ruptures or the L-film was lowered onto a submerged substrate by removing a part of the liquid subphase [19]. Transferred (LB) films are typically studied by tunneling and scanning electron microscopy (TEM) (SEM), atomic force microscopy (AFM), and grazing-incidence small angle X-ray scattering (GIXD). We note that only the latter technique provides reliable information on the long-range order of close-packed arrangements of MNPs.

Most common applications of LB-films of MNPs are photonic devices [26, 27] and substrates for surface enhanced resonance measurements [28–31]. One advantage of the LB method is that the electronic and magnetic interactions between MNPs can be altered by varying the average interparticle distances through variation of the surface pressure. Also tested has been the incorporation into bulk-heterojunction polymer solar cells [32], sensors for mercury detection [33] and organic acids and phenols [34], and catalysts for CO oxidation [35, 36].

8.2.2 LB-Films of MNPs Protected by Alkylamine and Alkylthiolate Ligands

MNPs, especially gold NPs, protected by a self-assembled monolayer of alkylthiolates or alkylamines have been most widely studied because of their relatively straightforward synthesis. With increasing length of the ligand's alkyl chains, these MNPs become increasingly hydrophobic since the partially charged surface of the metal core is better shielded from the outer surface of the MNP by longer alkyl groups. Still, even the most hydrophobic MNPs may form reasonably stable L- and LB-films if their size distribution is sufficiently narrow and their protective layer is adequately stable. However, the collapse pressures of their L-films were often small with values between 5 mN/m for weakly attached laurylamine ligands [23] and 15 mN/m for dodecanethiolate [37] on gold NPs. A change from dodecanethiolate to pentanethiolate protective ligands resulted in the expected decrease in surface area per NP from 11 to 6 nm^2 and a shorter distance between gold cores as confirmed by GIXD studies. Unexpected was the twice as high collapse pressure (30 mN/m) of the pentanethiolate protected gold NPs when compared to the dodecanethiolate protected NPs because ligands with longer alkyl chains generally provide a higher stability to the NPs. However, compressed monolayers of both gold NPs displayed the expected hexagonally close-packed arrangement at the air-water interface.

Similar values were reported by Medina-Plaza et al., Chen et al., and James et al. Medina-Plaza et al. generated LB monolayers of dodecanethiolate protected gold NPs on ITO electrodes for applications in electrochemical sensing [34]. They reported the formation and successful transfer of L-films of mostly hexagonally

close-packed gold NPs at a surface pressure of 10 mN/m and a surface area per MNP of 30 nm^2 for NPs with a diameter of 4.9 ± 0.5 nm. However, the L- and LB-films consist of small domain structures with no long-range order and frequent defect sites. Chen et al. deposited LB monolayers of dodecanethiolate protected gold NPs on ITO electrodes to enhance the efficiency of photovoltaic devices [32]. They reported similar optimum surface pressures of about 10 mN/m for the transfer of close-packed L-films of gold NPs of core diameters 3, 6, 10, and 16 nm. However, TEM images revealed many more defects, especially empty areas, for the LB films of the larger gold NPs (10 and 16 nm) than for the smaller MNPs. The authors also observed the often reported self-aggregation and island formation at low surface pressures.

James et al. utilized commercially available 4-*tert*-butylthiophenol protected gold NPs of 4.3 nm diameter with a standard deviation of 2.5 nm for the preparation of L- and LB-monolayers on quartz [33]. Close-packed films were obtained at a surface pressure of 15 mN/m while films with larger interparticle spacing were generated at a lower surface pressure of 8 mN/m. The less densely packed films were less sensitive for mercury vapour measurements by about 50 % but provided a faster mass flux of mercury. The authors also tested the heat stability of the films for thermal recovery and observed coalescence of gold NPs at 513 K to MNPs of about 8 nm diameter.

Changes in collapse pressure as observed for dodecanethiolate and pentanethiolate protected gold NPs may be caused by differences in size distributions but different degrees of crystallinity of the alkyl chains will also contribute to the observed differences. Thiolate ligands with alkyl chains of 12 or more carbon atoms usually generate crystalline domains of alkyl groups while shorter alkyl chains do not. So, alkylthiolate protected MNPs with shorter alkyl chains may be "softer" than those with longer alkyl chains, which is counterintuitive at first glance. In fact, a recent study on the chain length dependence of collapse pressures of alkylthiolate protected gold NPs confirmed increases in collapse pressure of more than 30 mN/m for the NPs with longer alkyl chains (Fig. 8.2) [38]. The authors could show that this is mainly an effect of the order-to-disorder (melting) transition of the alkyl chains. Alkyl chains with even numbered carbons of 14 or more are crystalline and generate L-films of much higher collapse pressure if the L-film studies are conducted at 22 °C.

Matsumoto et al. performed LB studies on almost monodisperse Au_{147} and Au_{55} NPs with hexylthiolate (NP diameter = 3 nm and core diameter = 1.8 nm) and octadecylthiolate ligands (NP diameter = 5 nm and core diameter = 1.3 nm), respectively [39]. Both gold NPs formed L-films that could be transferred onto TiO_2 (110) surfaces at surface pressures of 10 and 3 mN/m. TEM analysis of the films obtained at 10 mN/m revealed an ordered hexagonal packing over distances larger than 1 µm and interparticle distances in agreement with the sizes of the MNPs (Fig. 8.3a). However, investigations by scanning transmission microscopy (STM) clearly demonstrated the labile character of these films as NPs were moved and removed by the STM tip (Fig. 8.3b, c). The low density films transferred at 3 mN/m

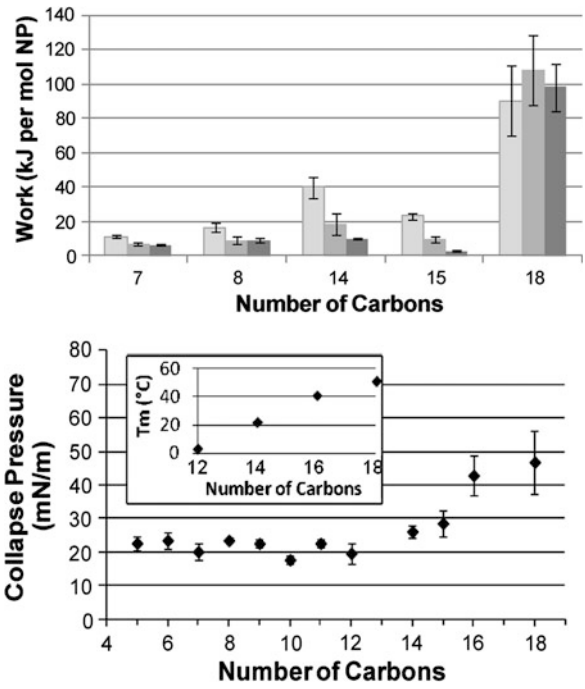

Fig. 8.2 *Top graph* Work required to collapse a monolayer of gold NPs protected by alkanethiols of different length at 13 °C (*left bar*), 22 °C (*centre bar*), and 40 °C (*right bar*). *Bottom graph* Collapse pressures of monolayers of gold NPs protected by alkanethiols of different length. Reprinted (adapted) with permission from [38]. Copyright 2012 American Chemical Society

were even more loosely packed and could not be studied by TEM and STM because of the high mobility of gold NPs on the surface.

In an early LB study, Heath et al. reported the formation of long-range hexagonally close-packed two-dimensional layers for alkylthiolate protected gold and silver NPs that have the right combination of core size and alkyl chain length if the size distribution is sufficiently small [40]. They proposed that the assembly of MNPs strongly depends on the amount of excess (conical) volume (V_e) available to the passivating ligands. For $V_e > 0.35$ nm^3, large interpenetration of the alkyl chains of adjacent particles generates extended one-dimensional structures at low surface pressures and two-dimensional foam-like phases at high pressures. Attractive dispersion forces between metal cores dominate for $V_e < 0.35$ nm^3 but are sufficiently reversible to generate long-range hexagonally close-packed two-dimensional layers of MNPs for V_e values larger than 0.15 nm^3. V_e values below 0.15 nm^3 result in the often observed irreversible self-aggregation of MNPs.

Clearly, the behavior of MNPs protected with alkylamines and—thiolates in L- and LB-films is complex because it depends on many different parameters such as size, size distribution, linking group, length of alkyl chain, spreading solvent, pH and temperature of subphase, and the ligand to gold ratio. An exact comparison of results reported by different groups may be possible if only one parameter changes but the preparation of two identical batches of monolayer protected MNPs is already a challenge due to synthetic limitations. However, the reliable and

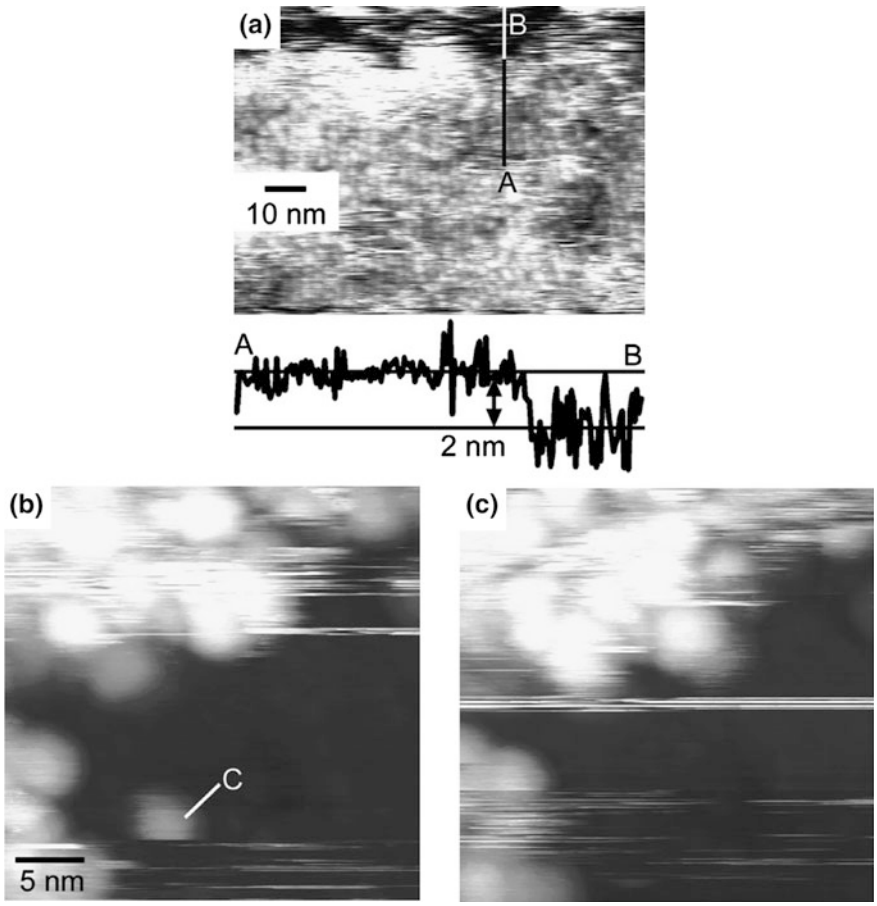

Fig. 8.3 **a** SEM image of hexagonal pattern of hexaylthiolate protected gold NPs on a TiO_2 (110) substrate. STM images of the same gold NPs on TiO_2 that reveal the removal of NP C in image (**b**) by the STM tip to give image (**c**) [39]. Reprinted from [39], Copyright 2007, with permission from Elsevier

reproducible preparation of layers consisting of hexagonally close-packed MNPs of long-range order, as required for many applications, does not seem to be feasible. A central problem is the self-aggregation of hydrophobic and most other MNPs at the air-water interface that generates floating islands of irreversibly associated MNPs. The glass-like rigid structure of these island phases prevent rearrangements of MNPs that are required for the formation of defect free films with long range packing order upon compression at the air-water interface. Many research groups chose the addition of a second spreading component, such as excess ligand, a surfactant, or just alkanes, as a versatile option to improve the interfacial properties of monolayer protected MNPs.

In a recent study, Gagnon et al. demonstrated that a simple addition of alkanes to gold NPs protected by tetradecylthiolate generates a liquid expanded phase of improved fluidity and reversibility as confirmed by compression–expansion hysteresis measurements [41]. The added alkane is assumed to be incorporated into the alkyl layer of the gold NPs to minimize the conical free volume of the ligand shell. This incorporation is reversible as the alkanes are assumed to be partially squeezed out upon compression. Particularly interesting is the reported dependence on temperature and length of the added alkane. In this study good mixing between the tetradecylthiolate protected gold NPs and an alkane only occurs at temperatures below the melting point of the alkyl chains attached to the MNP (order-to-disorder transition) and if the added alkane has at least the same number of carbon atoms as the alkyl group of the ligand. However, defect free films with long-range hexagonally close-packed order were not obtained and the addition of alkanes either lowered the collapse pressure or generated featureless pressure-area isotherms for all fluid liquid expanded films.

A unique approach to more stable L-films of alkylthiolate protected gold NPs was reported by Sanders et al. [42]. They added a solution of 1,12-dithioldodecane to L-films of alkylthiolate protected gold NPs with alkyl chains ranging from 6 to 18 carbon atoms at a low surface pressure of 0.2 mN/m. Expectedly, the L-films of MNPs with alkyl chain lengths of 6–14 carbon atoms had collapse pressures of below 15 mN/m, were rather disordered, and difficult to transfer as intact films. Addition of 1,12-dithioldodecane increased collapse pressures to values above 20 mN/m (Fig. 8.4), generated larger areas of close-packed order, and allowed a transfer by the LB and Langmuir-Schäfer techniques. This change in properties was reasoned with an apparent cross-linking of the MNPs at the air-water interface. Other evidence of cross-linking was provided by TEM images that revealed membrane like properties of the L-films (Fig. 8.5). In contrast, collapse pressures of gold NPs protected by hexa- and octadecylthiolates were larger than 30 mN/m and decreased upon addition 1,12-dithioldodecane and so did the degree of order of their assembly. This is not surprising as the dithiolate is much shorter than the interparticle distance between these MNPs and probably also does not easily insert into the more crystalline ligand layer of hexa- and octadecylthiolates.

8.2.3 LB-Films of MNPs Containing Polar Ligands

Another and more widely approach to L- and LB-films with larger collapse pressures is the addition of surfactant molecules or ligands with polar terminal groups to hydrophobic alkylthiolate and alkylamine protected MNPs. Experimentally most straightforward is the co-deposition of hydrophobic MNPs protected by outer alkyl groups with an amphiphilic compound. Swami et al. showed that laurylamine protected gold NPs do not form stable L-films and are not amenable to transfer onto substrates [23]. Addition of water insoluble octadecanol to the spreading solution of laurylamine protected gold NPs significantly improved the amphiphilicity and

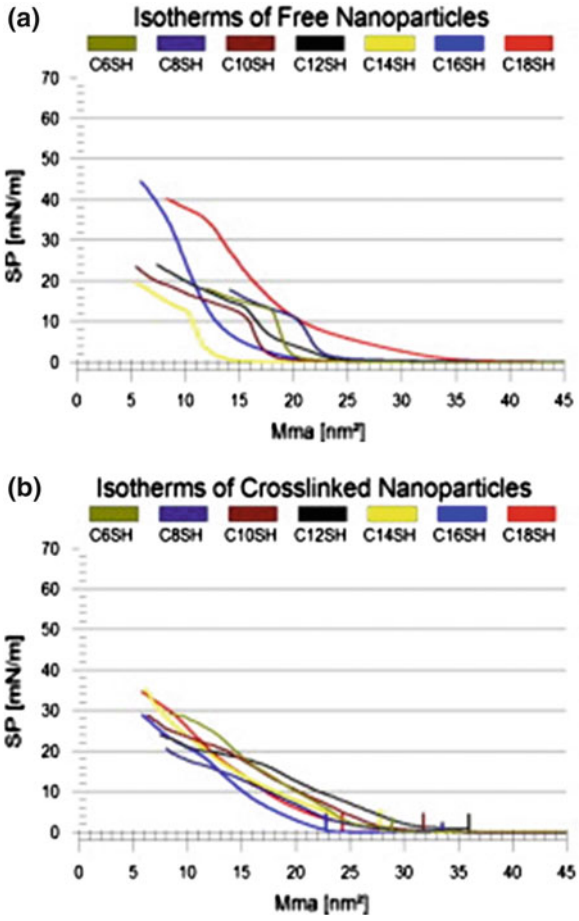

Fig. 8.4 Pressure-area isotherms of **a** free and **b** crosslinked gold NPs protected by alkylthiols of different length [42]. Reprinted from [42], Copyright 2014, with permission from Elsevier

stability of the L-film that could now be transferred onto substrates to form mono- and multi-layer LB-films. Unfortunately, large increases in surface pressure over time after spreading and surface areas per cluster that were four times the maximum estimated area indicated structural rearrangements of the MNPs. This assumption was corroborated by a comparison of TEM images of as prepared laurylamine protected gold NPs and after their deposition as LB monolayer that revealed an overall increase in size and in size distribution of the gold cores from initially 5 (±0.5) nm to 8–28 nm. Clearly, the weakly attached laurylamine ligands do not provide sufficient stability for LB studies and probably rearrange and exchange in the presence of octadecanol. The increased area per cluster are likely generated by areas just covered with octadecanol as the amount of octadecanol that inserts into the alkyl layer of the gold NPs is limited and will likely change with surface pressure.

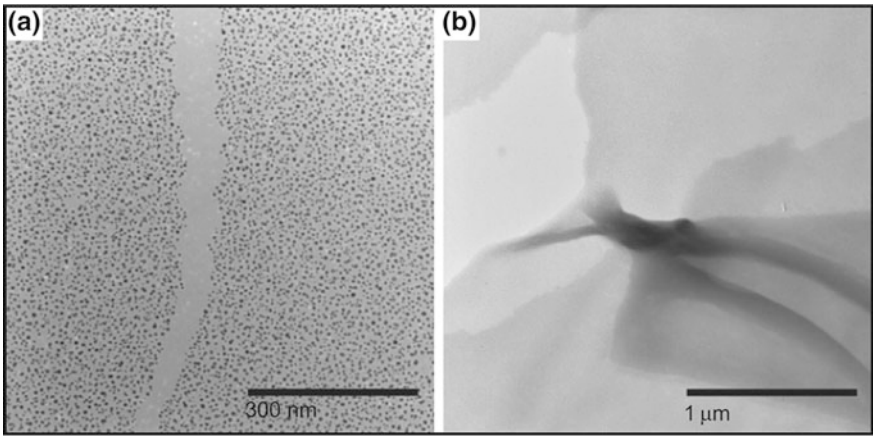

Fig. 8.5 High (**a**) and low (**b**) resolution TEM images of crosslinked hexanethiol protected gold NP that reveal uniform particle distribution, symmetric tears, and possible folding of the flexible film. Reprinted from [42], Copyright 2014, with permission from Elsevier

Bjørnholm and co-workers conducted a comparable study with more stable alkylthiolate protected gold NPs and, perhaps more importantly, they added the amphiphilic compound as a functionalized alkylthiolate to generate gold NPs with two different types of ligands (e.g. dodecanethiolate and 11-hydroxyundecanethiolate) [37]. The most important outcome of these studies is that the randomly attached thiolate ligands are sufficiently mobile to rearrange at the air-water interface. Amphiphilic Janus type gold NPs are generated since most of the ligands bearing terminal hydroxyl groups migrated so that they face the aqueous phase (Fig. 8.6). Expectedly, the collapse pressures of their L-films increased from 15 mN/m for just dodecanethiolate ligands to over 30 mN/m for a 5:1 mixture of dodecanethiolate and 11-hydroxyundecanethiolate. The authors also could show by GIXD studies that entirely hydrophobic gold NPs protected by a mixture of dodecanethiolate and pentanethiolate also respond to the interfacial conditions by generating more elongated NPs when compressed as L-film. The observed packing distances agree with an expulsion of the long-chain ligands from the plane of the monolayer as a response to the increased surface pressure. Similar rearrangements of ligands have also been observed in self-organizing MNPs discussed later.

Most widely applied has been the addition of amphiphilic molecules that likely add a second layer of ligands by interdigitation of the aliphatic chains. In the simplest case, it is the addition of excess ligand as recently reported by Lau et al. [43]. They prepared nearly monodisperse gold NPs of 8.0 nm core diameter that were protected by a monolayer of oleylamine. These NPs do not form defect free monolayers at the air-water interface because of their strong tendency to aggregate. Addition of an extra amount of oleylamine diminished self-aggregation so that L- and LB-films of long-range hexagonally close-packed order were obtained

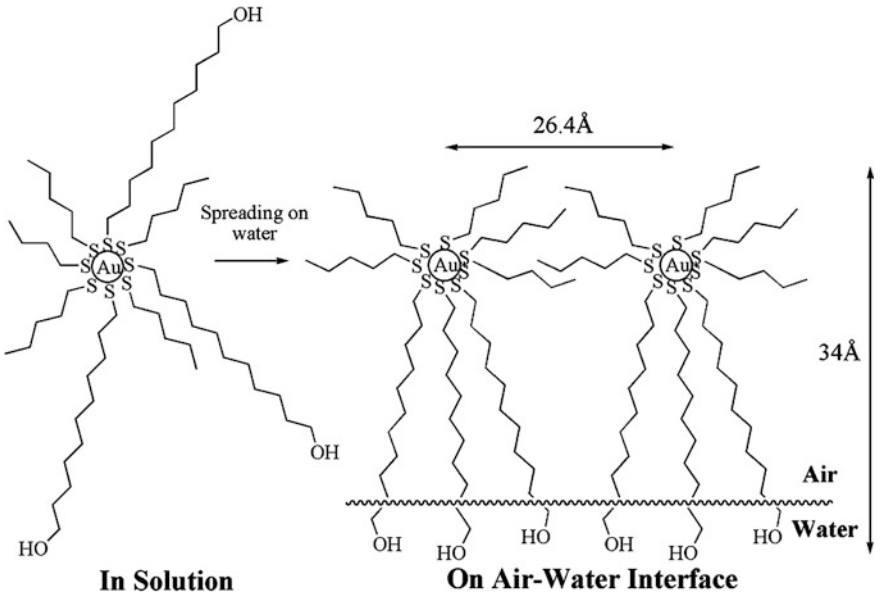

Fig. 8.6 Randomly attached alkylthiolate and 11-hydroxyundecanethiolate ligands rearrange on a gold NP surface to generate amphiphilic Janus-type NPs at the air-water interface. Reproduced from [37] with permission of The Royal Society of Chemistry

(Fig. 8.7). It is assumed that the extra amount of oleylamine attaches to the NPs so that their aliphatic chains mix (interdigitate), which generates amine and ammonium groups at the outer surface of the gold NPs. Amine groups provide a better interaction with the aqueous phase while ammonium groups prevent strong self-aggregation due to charge repulsion. Notably, the excess oleylamine may also be added to compressed L-films of oleylamine protected gold NPs that already contain multilayers and other defects to generate L-films of similar long-range hexagonally close-packed order described above (Fig. 8.8).

An elegant approach to the synthesis of surfactant protected silver NPs was presented by Lee et al. [44]. They reported the formation of stearate protected silver NPs by thermal decomposition of a multilayer film of silver stearate at 550 K. The obtained MNPs of 4 nm diameter readily form monolayer assemblies at the air-water interface with an astonishing collapse pressure of 59 mN/m, which is higher than for a monolayer of just stearate molecules. The high stability of the NP monolayer is reasoned with significant interdigitation between the alkyl chains of stearate ligands on adjacent silver NPs. Interdigitation between ligands was supported by interparticle distances of 3–3.5 nm measured by TEM, which was 0.5–1.0 nm smaller than the predicted diameter based on the length of stearate ligands (Fig. 8.9). Also successful was the transfer of these stearate protected silver NPs onto substrates by the LB technique.

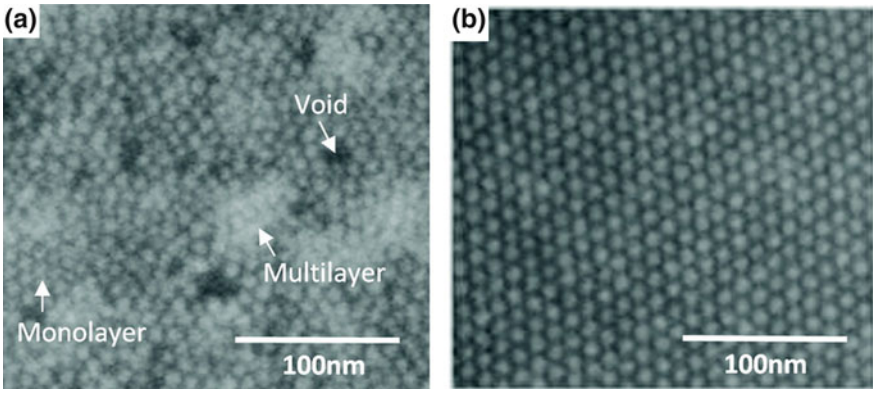

Fig. 8.7 SEM images of LB films of oleylamine protected gold NPs transferred onto silicon substrates without (**a**) and with excess oleylamine (**b**). Reprinted (adapted) with permission from [43]. Copyright 2012 American Chemical Society

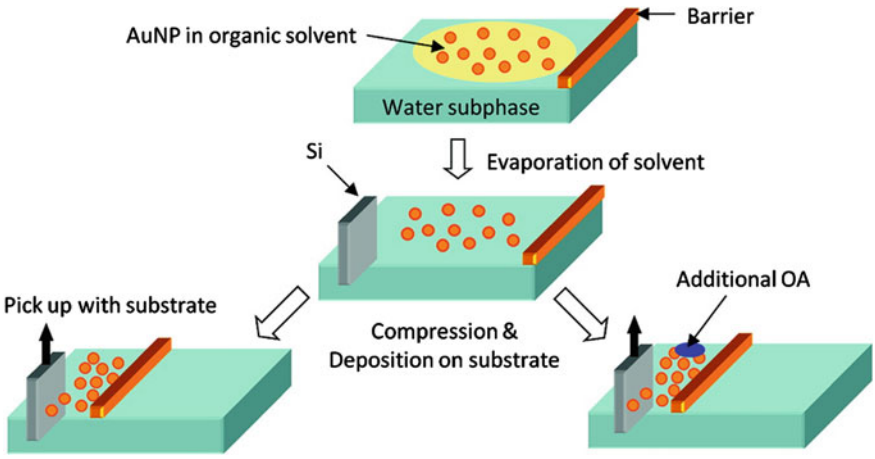

Fig. 8.8 LB assembly process of oleylamine protected gold NPs with and without addition of excess oleylamine (OA) [43]. Reprinted (adapted) with permission from [43]. Copyright 2012 American Chemical Society

Similarly, the addition of fatty acid ω-tricosenoic acid to mercaptoaniline protected palladium NPs significantly improved their interfacial properties [45]. L-films of the pure mercaptoaniline protected palladium NPs with a core diameter of 1.5–2.0 nm collapsed at surface pressures larger than 6 nm/m but assembled into a monolayer at very low pressure of 2 mN/m. Addition of ω-tricosenoic acid to the spreading solution increased the film's robustness to a surface pressure of 30 mN/m and these mixed L-films could be readily transferred by vertical dipping while the pure monolayer could only be transferred horizontally by trough draining.

Fig. 8.9 TEM image of stearate protected silver NPs obtained by thermal decomposition of a multilayer film of silver stearate at 550 K [44]. Springer and the original publisher/The European Physical Journal D-Atomic, Molecular, Optical and Plasma Physics, 16, 2001, 293–296, Phase Behavior of organic-inorganic crystal, S.J. Lee, S.W. Han, H.J. Choi, and K. Kim, Fig. 8.3, original copyright notice) with kind permission from Springer Science and Business Media

A comparison of the surface areas per entity of the pure components and the mixture as well as IR studies agree with a side-by-side arrangement of palladium NPs and ω-tricosenoic acid in the L- and LB-films and no significant H-bonding between the aniline and carboxylic acid groups.

8.2.4 LB-Films of MNPs Protected by Ionic Surfactants

Ionic surfactants have also been used as additives, which allows for a combined application of electrostatic assembly with the LB technique. In addition, these MNPs are more biocompatible especially if fatty acids and amines or other chargeable biomolecules are incorporated. Sastry et al. generated MNPs with an outer layer of carboxylic acid or amine groups by adding neutral fatty acid or amine molecules to alkylthiolate protected silver and gold NPs [9, 46]. At carefully controlled conditions interdigitation between aliphatic chains of the fatty acid or amine and the alkyl groups of the ligands results in the formation of a bilayer. This phenomenon appears to be unique to NPs as a similar bilayer formation is not observed for self-assembled monolayers of alkylthiolates on flat silver and gold surfaces, probably because of insufficient free volume. At pH = 9 a carboxylic acid terminated bilayer MNP is charged and dissolves in the aqueous subphase but

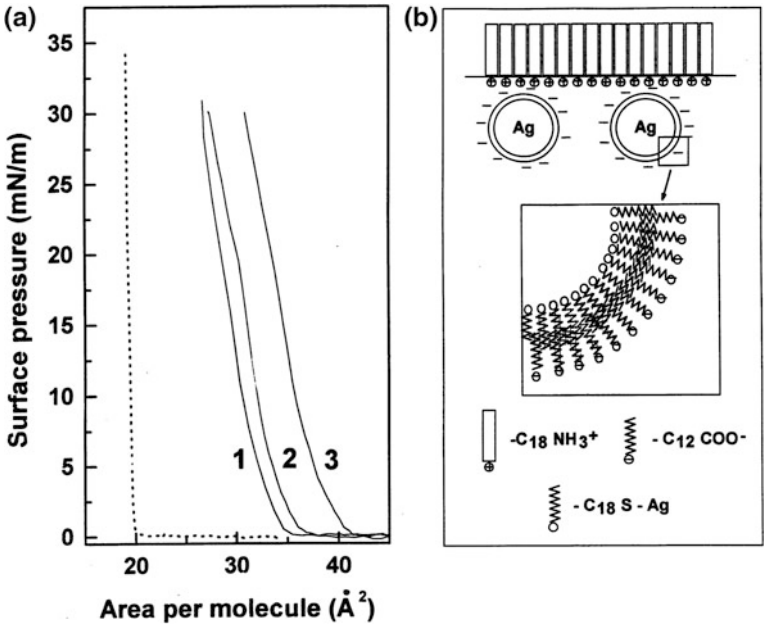

Fig. 8.10 **a** Pressure-area isotherms of octadecylamine before and after the exposure to lauric acid protected silver NPs dissolved in the aqueous subphase for 15 min (*Line 1*), 60 min (*Line 2*), and 120 min (*Line 3*). **b** Cartoons of the octadecylamine L-film after exposure to lauric acid protected silver NPs and the proposed interdigitated bilayer of lauric acid on the surface of the silver NPs [9]. Copyright 1998 American Chemical Society

attaches electrostatically to an oppositely charged L-film of fatty amines that are also charged at this pH (Fig. 8.10). Obviously, amine and acid groups may also be exchanged and oppositely charged MNPs may also be used for electrostatic assembly. Complex multilayers were generated at the air-water interface by alternating addition of oppositely charged species, including single-stranded DNA and other charged biomolecules, to the aqueous subphase. Transfer of these electrostatically assembled multilayer L-films onto substrates is possible but the authors also highlight other processing options based on thermally evaporated fatty lipid films. We note that these charged MNPs may also be processed by electrostatic layer-by-layer deposition without the help of the LB technique as described later.

Cationic monomeric and gemini imidazolium surfactants were studied as protective ligands for silver NPs by Datta et al. [47]. Since the NPs were synthesized in aqueous solution it is assumed that polar imidazolium groups point towards the silver surface and towards the water phase to generate bilayers around the NPs. This structure probably remains unchanged upon transfer into chloroform as spreading solvent. The spacer length between imidazolium units in the gemini structures proved to be an important parameter as it affects the shape of the formed silver NPs and the order of the aggregates generated at the air water interface (Fig. 8.11). All

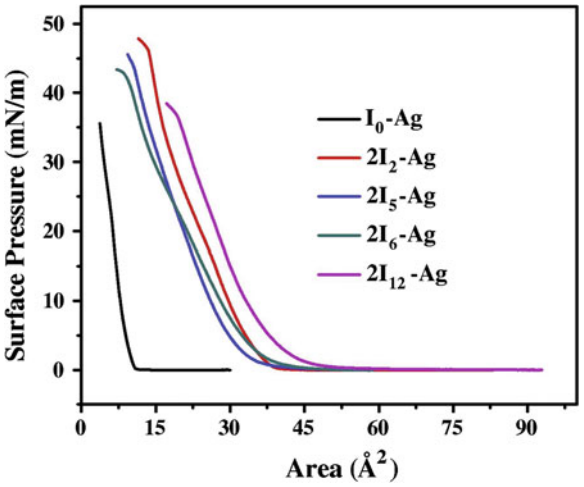

Fig. 8.11 Pressure-area isotherms for silver NPs protected with monomeric (I_0) and gemini imidazolium surfactants of varying spacer length (2–12 carbon atoms) at 28 °C. On average, an area of 40 ± 5 Å per silver NP protected by gemini surfactants is obtained for the extrapolated onset of surface pressure [47]. Reprinted from [47], Copyright 2014, with permission from Elsevier

silver NPs display the gas-analogous state at low pressures, the liquid-condensed phase at intermediate pressures, and a solid-analogous phase at high pressures, which is ideal for the formation of long-range ordered assemblies. However, especially silver NPs protected by gemini imidazolium surfactants with shorter spacers already self-aggregate at low surface pressures to generate islands of condensed phases of close-packed structures. AFM images of LB films confirmed the presence of islands and multilayer assemblies.

Charges may also be attached to MNPs via charged protective ligands. Sashuk et al. prepared gold and silver NPs that were protected by a mixture of two ligands [48]. One ligand was the hydrophobic 1-undecanethiol and the other ligand contained a charged or chargeable end group, such as 11-mercaptoundecyltrimethylammonium chloride and 11-mercaptoundecanoic acid. Attachment in solution should give a rather random distribution of the two ligands but the ligands are expected to rearrange at an air-water interface with the charged ligands facing the water surface. Similar rearrangements of polar and apolar thiolate ligands were reported by Bjørnholm and co-workers and described above [37]. To ensure insolubility in water not more than 15 % of the ligands per NP can be charged, which is sufficient to generate amphiphilic MNPs that form stable L- and LB-films (Fig. 8.12). Surprisingly, cationic MNPs with ammonium end groups gave higher ordered and more stable two-dimensional assemblies than anionic MNPs with carboxylic acid. For example, cationic MNPs withstood surface pressures of 40 mN/m whereas L-films of anionic MNPs already collapsed at 25 mN/m. This difference is explained with strong H-bonding between remaining carboxylic acid

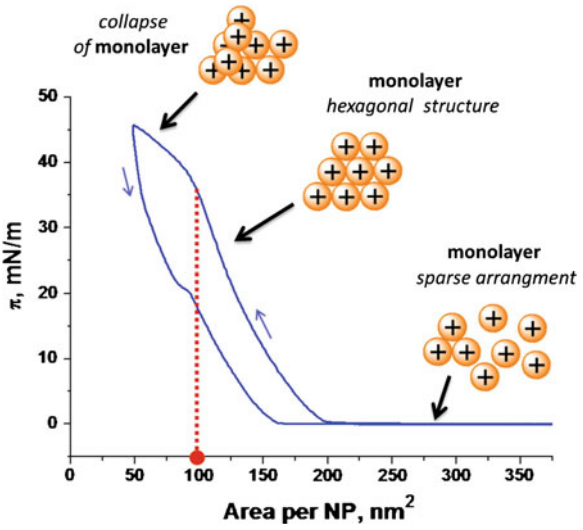

Fig. 8.12 Pressure-area isotherms on compression and expansion for positively charged MNPs with an onset of surface pressure at a surface area of about 200 nm^2/NP. The observed hysteresis is reasoned with a migration of MNPs into the aqueous phase [48]. Reprinted from [48], Copyright 2012, with permission from Elsevier

groups at the MNP's surface. However, long-range order of hexagonally close-packed NPs was neither achieved with cationic nor with anionic MNPs even though the former generated significantly larger defect-free domains.

8.2.5 L- and LB-Films of MNPs Protected by Polymers

Protection by MNPs by a polymer layer rather than ligand molecules usually increases the stability of the MNPs and their overall size because polymer layers tend to be thicker, denser, and less uniform than self-assembled monolayers of molecular ligands. A comparative study on gold NPs protected by a molecular surfactant oleylamine, which probably forms a partial bilayer, and poly(vinyl pyrrolidone) (PVP) was provided by Benkovičová et al. [49]. Unfortunately, the core sizes and size distributions of the two samples were significantly different with core diameters of 14.6 (±15) and 24.4 (±20) nm for oleylamine and PVP, respectively, although the thickness of the organic layer was almost identical with 0.7 and 0.8 nm, respectively. Nevertheless, both samples of gold NPs assembled into hexagonally close-packed arrays of relatively long-range order as LB-films on silica substrates and, more surprisingly, by drop casting onto silica substrates (Fig. 8.13). Clearly, the lower polydispersity of the oleylamine protected gold NPs is the main reason for the generation of more ordered self-assembled arrays. The authors do not mention any problems with self-aggregation of these comparatively large MNPs.

Polyvinylpyrrolidone was also used as protective layer for rhodium NPs (nanocrystals) by Zhang et al. [50]. L-films were deposited onto silicon wafers by the Langmuir-Schäffer method at different compression pressures. TEM analysis of

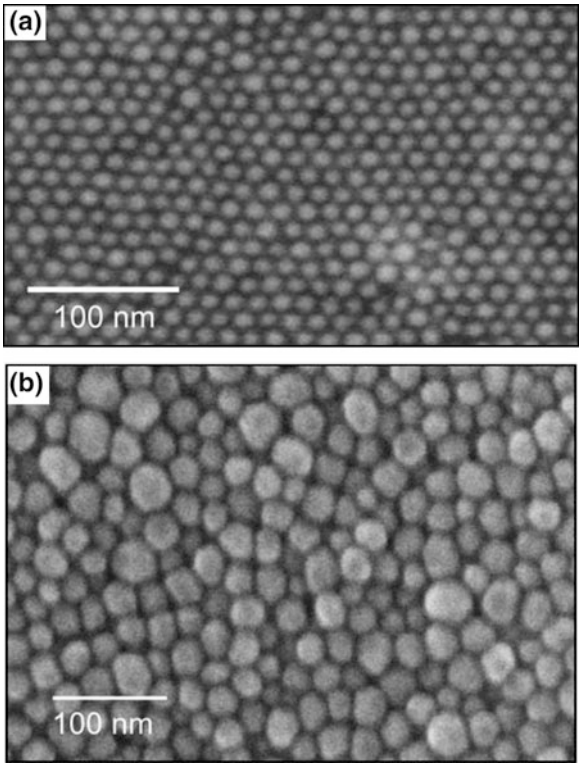

Fig. 8.13 SEM images of monolayers of gold NPs protected by oleylamine (**a**) and polyvinylpyrrolidone (**b**) obtained by drop casting onto silica substrates [49]. Springer and the original publisher, Chemical Papers, Preparation of sterically stabilized gold nanoparticles for plasmonic applications, 67, 2013, 1225–1230, Monika Benkovičová, Karol Végso, Peter Šiffalovič, Matej Jergel, Eva Majková, Štefan Luby, Alexander Šatka) with kind permission of Springer Science+Business Media

the monolayer LB-films revealed a constant increase in surface coverage with increasing surface pressure (11, 24, and 33 % at 4.4, 8.1, and 10.4 mN/m, respectively) in Fig. 8.14a. Buckling of the L-film to multilayers was observed at a surface pressure of 12.9 mN/m in Fig. 8.14b. However, smaller sized particles (6.5 and 8.3 nm in diameter) showed higher surface coverage than larger particles (13.5 nm) when compression pressures below 10 mN/m were applied, which was reasoned with a lower polydispersity of the smaller rhodium NPs. At surface pressures greater than 10 mN/m the samples showed large deviations in surface coverage (35–64 %) that are likely caused by the different geometric shapes of the formed rhodium nanocrystals. Interestingly, all tested LB-films showed catalytic activity for the hydrogenation of ethylene, which confirmed that active surface area was available on the rhodium NPs despite the polymer coating.

A rather unique approach was chosen by Genson et al. who attached an amphiphilic V-shaped polymer to gold NPs [51]. The structure of the attached ligand containing a hydrophobic polybutadiene chain and a hydrophilic poly(ethylene glycol) chain is given in Fig. 8.15a. These ligands were not attached by ligand

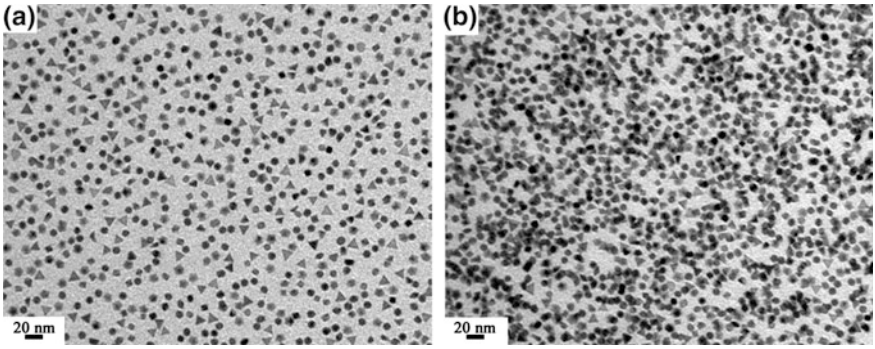

Fig. 8.14 TEM images of LB films of 8.3 nm Rh nanocrystals transferred at surface pressures of **a** 10.4 mN/m (monolayer) and **b** 12.9 mN/m (multilayer). Reprinted (adapted) with permission from [50]. Copyright 2007 American Chemical Society

exchange or during the formation of the MNPs but via an esterification of mercaptophenol protected gold NPs of 2 nm diameter to generate a dense organic layer. Due to their amphiphilic coating the MNPs spread well at the air-water interface with an onset of surface pressure at a surface area of 200–250 nm^2/MNP and a minimum area of 30 nm^2/MNP before collapse at a surface pressure of 18 mN/m. Compression was reversible and a condensed monolayer was obtained at a surface area per MNP of 140 nm^2. Comparison of the measured areas per MNP in the L-films and AFM studies on LB-films suggest a dissolution of most poly(ethylene glycol) chains in the aqueous subphase upon compression and a preferential arrangement of the polybutadiene chains at the air-water interface to generate MNPs of pancake-shape (Fig. 8.15b).

Tao et al. demonstrated that much larger MNPs can also be processed into LB-films of long-range order [52]. They prepared silver NPs (nanocrystals) of diameters of 100–250 nm and different polyhedral shapes that were protected by PVP. Transfer onto silicon wafers was accomplished at different surface pressures between 0 and 14 mN/m to change plasmonic properties by changing average interparticle distances from 40 nm to about 2 nm, respectively. Related work with PVP protected silver and gold NPs, nanocubes and nanocages, respectively, was reported by Mahmoud et al. [27]. Their MNPs were smaller in size with diameters of about 75 nm and surface pressure well above 30 mN/m could be reached before the L-films collapsed. However, LB-monolayers with uniform distribution of MNPs were obtained only at low particle density and with MNPs that contained only very small amounts of free PVP. Even smaller are the PVP protected platinum NPs reported by Song et al. with sizes of about 10 nm [26]. Samples with primary cubic, cuboctahedral, and octahedral shapes generated LB monolayers of similar order. However, surface pressures as low as 6 mN/m already generated LB-films with MNPs escaping into the third dimension.

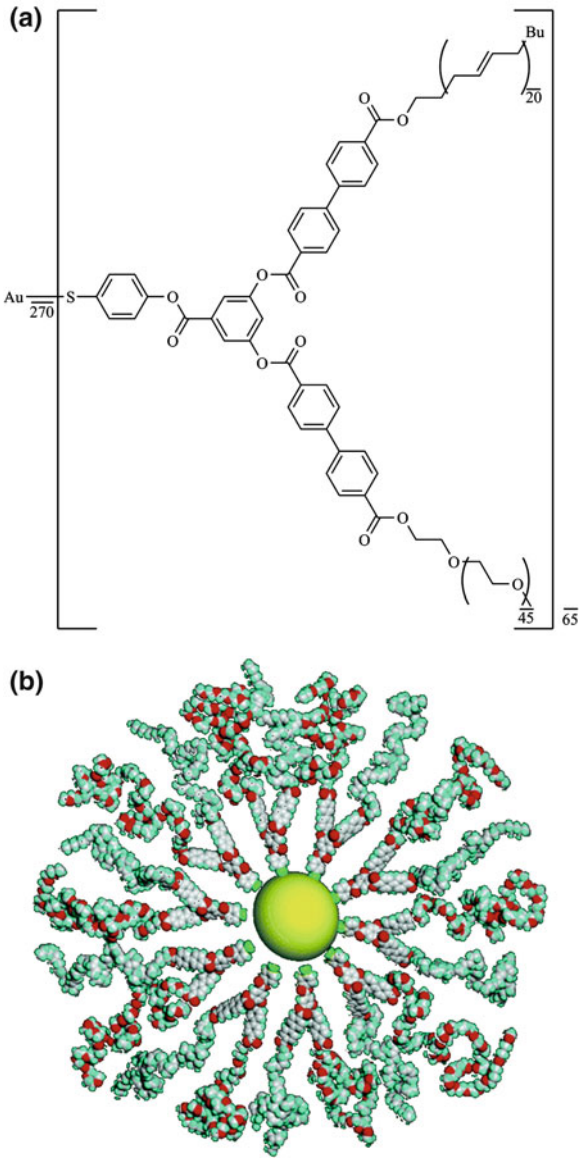

Fig. 8.15 **a** Chemical structure of a monomer unit of the V-shaped ligand $(PB\text{-}PEG)_n$ and **b** a simplistic molecular model of a gold NP coated with ten V-shaped ligands that have poly (ethylene glycol) chains in an amorphous state. Reprinted (adapted) with permission from [51]. Copyright 2006 American Chemical Society

8.2.6 L- and LB-Films of Magnetic MNPs

Many properties of magnetic MNPs also depend on their size, size distribution, and types of protective ligands as discussed above but we decided to grant them a separate part because of their unique magnetic interactions and properties. Magnetic dipole-dipole interactions may affect their assembly in L- and LB-films if the MNPs

have sufficiently large volumes and high magnetic moments. Magnetic dipolar interactions one order of magnitude stronger than the thermal energy of MNPs at room temperature have been reported as well as precipitation of 14 nm cobalt NPs due to too strong magnetic interactions. We refer to a recent review by Bellido et al. for more details on magnetic interactions and the processing of magnetic NPs in general [53]. Reviewed in the following are L- and LB-films of MNPs, not including metal oxide NPs, which reduces the number of examples to sufficiently air stable iron and cobalt containing NPs.

L- and LB-films of iron/platinum NPs have been reported by two groups. Wang et al. prepared iron/platinum NPs protected by oleic acid and oleylamine with a core diameter of 4 nm and a standard deviation of less than 10 % [54]. These mainly hydrophobic MNPs generated close-packed assemblies at the air-water interface and could be transferred onto substrates at surface pressures between 15 and 20 mN/m that equal a surface area per MNP of 60–70 nm^2. Unique of this study is the comparison of LB-film formation on substrates of different hydrophilicity according to surface contact angle measurements. Intact LB monolayers of close-packed MNPs were obtained only on substrates with contact angles of water larger than 65°, which is considered as the boundary between hydrophobic and hydrophilic behavior.

Less successful were Wen et al. with their attempt to generate LB films with 3–4 nm iron/platinum NPs protected by PVP [55]. Although pressure-area isotherms reveal high collapse pressures of larger than 50 mN/m for L-films of pure MNPs and their mixture with stearic acid, their transfer onto carbon-coated copper TEM grids generated discontinuous films with multilayer areas. We assume some of these feature are already present in the L-film and generated by the transfer process, which suggests the MNPs self-aggregate relatively strongly. This conclusion, however, is contrary to what the authors concluded.

Thorough LB studies with relatively air-stable cobalt NPs protected by tridodecylamine were presented by Johans et al. [19]. They illustrate the importance of Brewster Angle Microscopy measurements in conjunction with pressure-area isotherms to identify self-aggregation and island formation of the MNPs. Contrary to several reports on surfactant supported L-film formation discussed above, the authors concluded from careful comparative studies that the presence of excess tridodecylamine (cobalt NPs were not repeatedly washed to remove all excess tridodecylamine) does not aid the spreading of cobalt NPs but tridodecylamine competes for surface area and promotes self-aggregation that even led to the precipitation of aggregates of cobalt NPs from the interface. Most likely, the steric bulk of tridodecylamine makes it much less useful as amphiphilic additive when compared to conventional fatty acids and amines. Another interesting result is the observation that the MNPs spread much better and more reversibly on ethylene glycol than on water because of its lower polarity and surface tension. The authors also compared different spreading solvents (chloroform, toluene, and hexanes) that affected the types of self-aggregates that are formed (Fig. 8.16) but all these measures did not generate close-packed L-films that could be transferred onto substrates. The best quality L- and LB-films were obtained from mixtures of

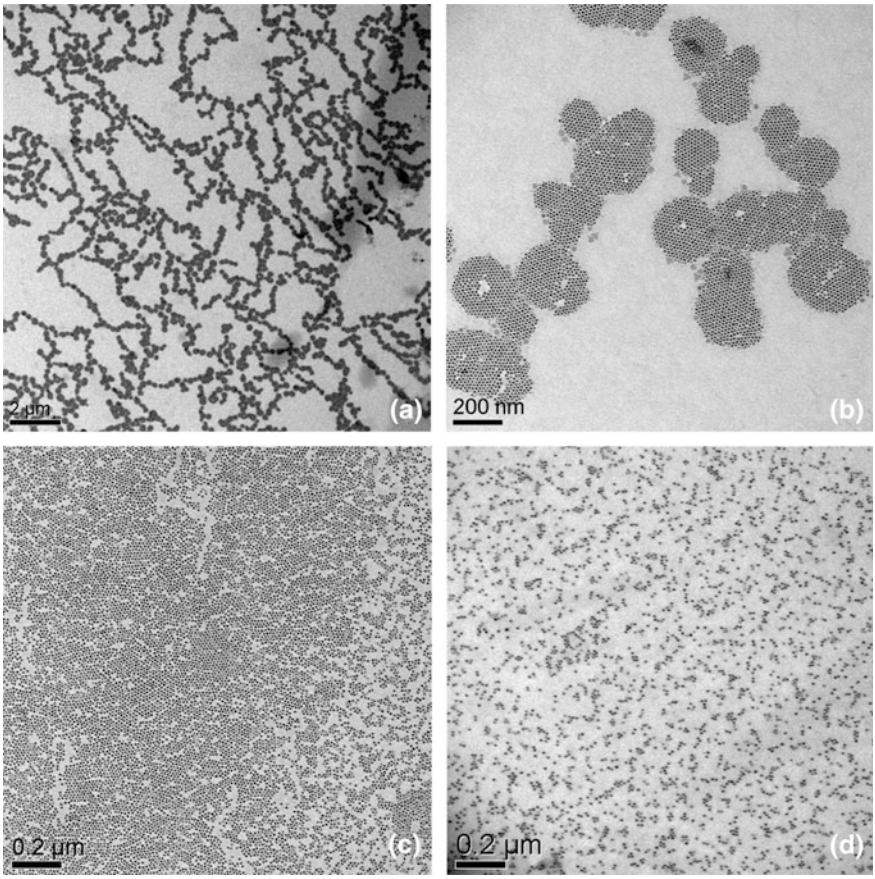

Fig. 8.16 TEM images of self-aggregated tridodecylamine protected cobalt NPs nanoparticles on ethylene glycol after evaporation of hexane (**a**, **b**) or toluene (**c**, **d**) solutions. Reprinted (adapted) with permission from [19]. Copyright 2010 American Chemical Society

tridodecylamine protected cobalt NPs with a block co-polymer PS-*b*-PEO on ethylene glycol as subphase. These films displayed superparamagnetic behavior at room temperature.

MNPs of cobalt alloys were studied in the groups of Singla [56] and Weller [24]. Singla and co-worker synthesized cobalt/nickel NPs of 8 nm diameter and reasonably small size distribution that were stabilized by PVP. Good quality L- and LB-films (up to six layers) were obtained when the spreading solution contained stearic acid and films were vertically transferred at a surface pressure of 30 mN/m and area per NP of 60–70 nm^2. AFM images of bilayers transferred onto glass slides are in agreement with a transfer of overall smooth, close-packed monolayers but some larger aggregates were also present. Weller and co-workers investigated 8 nm cobalt/platinum NPs of spherical and cubic shapes that were protected by

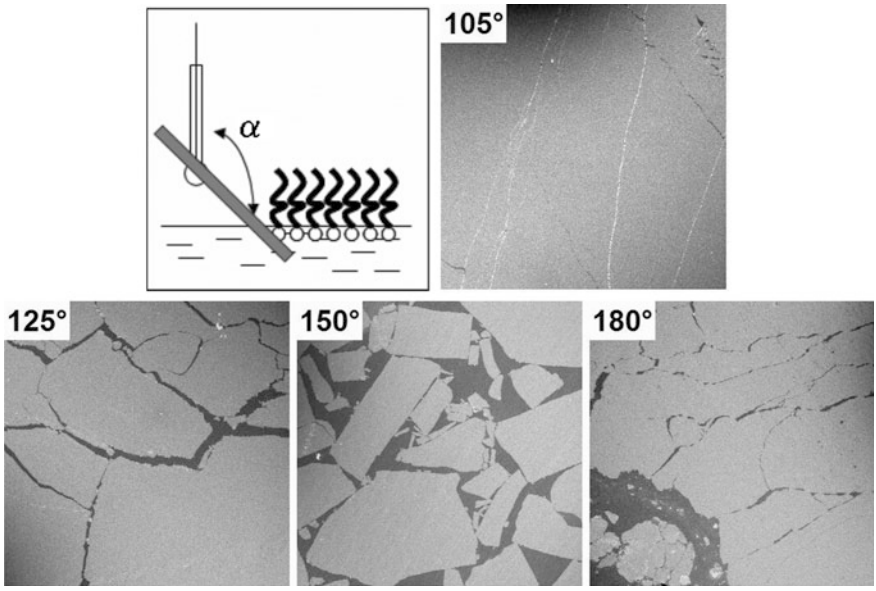

Fig. 8.17 SEM images of cobalt-platinum NPs monolayers transferred onto silicon wafers at various dipping angles. Light areas represent coverage by NPs while dark areas are uncovered by NPs. Reprinted (adapted) with permission from [24]. Copyright 2008 American Chemical Society

hexadecylamine. Essential for the formation of close-packed and relatively defect free L-films was a careful removal of excess hexadecylamine to avoid the formation of double layers of nanoparticles at domain boundaries and improve dispersion at the interface. The authors also demonstrated that good quality monolayers were formed on the less polar diethylene glycol but not on water as subphase, which seemed to be generally true for hydrophobic MNPs. The optimum surface pressure for transfer was determined to be 8 mN/m and a surface area per NP of 30 nm^2. Finally, they reduced the number of defects in transferred films by optimizing the dipping angle to 105°, in between vertical and horizontal transfer (Fig. 8.17).

8.2.7 LB Multilayers of MNPs

Most of the work presented above is focused on the preparation of monolayers whereas Kundu et al. presented some interesting results on the preparation of LB multilayers with dodecanethiol protected gold NPs of core diameters of 1.4 and 3.4 nm [57–59]. They succeeded in the formation of multilayers by sequential transfer of monolayer L-films onto H-terminated Si(001) substrates by vertical down-up cycles (LB method) at a surface pressure of 8 mN/m. To their surprise only odd numbered multilayers were generated, which they reasoned with a change

from Z-type to Y-type LB deposition after the first down-up cycle. In other words, no monolayer is deposited at the first down stroke but only at the first up-stroke. To reason this finding the authors hypothesized that the Si(001) substrate required some pre-wetting before deposition of gold NPs occurred.

Perhaps more surprising is that the authors apparently generated multilayer L-films by a simple increase in surface pressure beyond the collapse pressure of the monolayer. They reported the irreversible formation of bi-, tri-, and tetralayer films at surface pressures of 16, 21, and 25 mN/m, respectively. X-ray diffraction investigations of multilayer films transferred onto Si(001) substrates revealed some ordering of the MNPs and an unusually short interparticle distance between layers that suggested a strong interpenetration. However, the exact structures of the multilayer films remain unclear and, more importantly, are not stable over time. All multilayer films collapse over months into a monolayer of randomly assembled gold NPs of various but increased sizes [59]. Clearly, the close-packing of the gold NPs compromises their stability towards coalescence. The authors also show that the kinetic and mechanism of the collapse of the multilayer films depends on the chemical nature of the substrate surface by investigating the process not only on H-terminated Si(001) substrates but also Br- and HO-terminated Si(001) substrates [58].

8.3 Layer-by-Layer Deposition of Metal Nanoparticles

8.3.1 Introduction

Charged and uncharged MNPs may also be processed into thin films by a process called Layer-by-Layer (LbL) deposition that is somewhat related to the formation of LB-films but does not provide a direct control over the packing order and density within each layer. The method typically relies on electrostatic interactions between oppositely charged compounds, although examples that utilize H-bonding and other intermolecular forces have also been reported [60], and was initially developed for the LbL deposition of polyelectrolytes. However, many other molecular species have been incorporated into these multilayer films over the past two decades including charged MNPs and other colloidal particles [61–63]. In fact, the first reported electrostatic LbL deposition was actually utilizing colloidal particles and not polymers [64]. Charged MNPs are well suited for this technique because only a fraction of the attached charged groups can interact with the oppositely charged surface to leave a sufficient number of charges for the deposition of the next, oppositely charged layer. In other words, a non-stoichiometric excess of charged groups is deposited with each new layer relative to the preceding layer.

The generic process of LbL deposition is rather straightforward and illustrated in [65]: (a) A charged substrate is dipped into a solution containing oppositely charged material which will bind to the substrate. (b) The coated substrate is taken out of

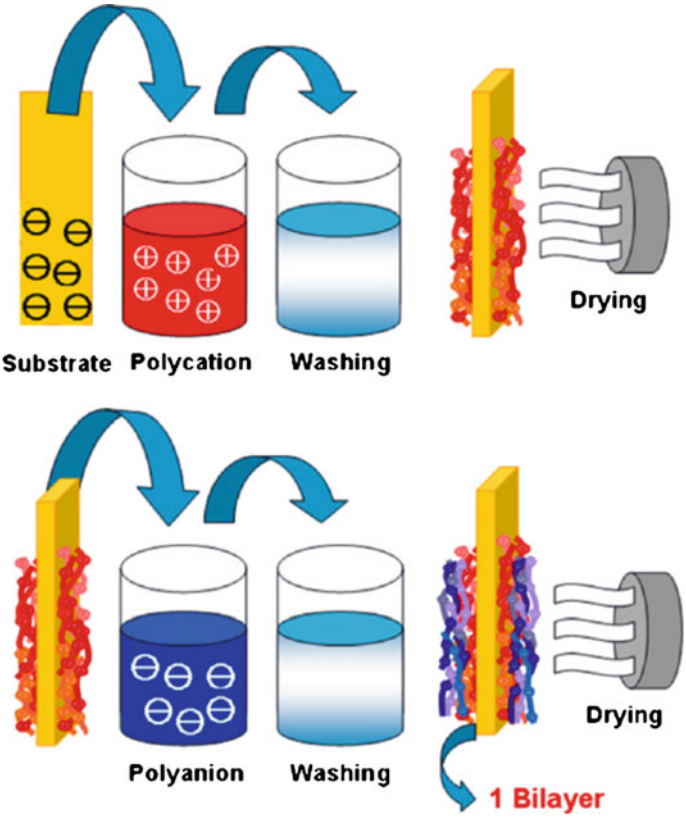

Scheme 8.1 Simplified cartoon of LbL assembly procedure driven by electrostatic attraction between adjacent films [65]. Reprinted from [65], Copyright 2010, with permission from Elsevier

solution and washed with solvent to remove excess material. (c) The substrate is then dried in air or a flow of inert gas to remove most solvent from the washing step. (d) The coated substrate is now immersed into a solution of an oppositely charged material to form the next layer on top. (e) The generated bilayer is again washed with solvent and dried before the process is repeated to build up multilayer films (Scheme 8.1).

One of the main attractions of the LbL method is its technical simplicity and applicability to many different types of surfaces but the apparent straightforward coating process may be deceptive since a range of different parameters must be taken into account to control the structural outcome. Important factors and properties that affect the structure of the formed LbL layer are the physical properties of the poly-charged species (e.g. elasticity and surface roughness), surface charge density, ionic strength and concentration of the solutions, the timeframe of adsorption, and the rinsing and drying process [66]. Each of these properties must

be optimized and accurately monitored to reproducibly generate the desired structure by LbL deposition.

Characterization of the generated LbL films depends on the same spectroscopic and diffraction methods as the characterization of LB-films. The lack of pressure-area isotherms and known exact amount of deposited compounds is often compensated for by quartz-crystal microbalance measurements.

8.3.2 LbL Deposition of Ionic MNPs

Ionic MNPs have been generated by the attachment of ionic ligand molecules, ionic dendrimers, and polyelectrolytes and have been deposited either as alternating layers of anionic and cationic MNPs or, more often, as alternating layers with oppositely charged polyelectrolytes. In all these cases electrostatic interactions dominate the LbL deposition and the structure of the resulting multilayer films depends on several processing parameters such as pH and ionic strength of the coating solutions and exposure time. However, highly ordered arrangements of MNPs, as achievable with the LB method, have rarely been generated by the LbL method. Also, in-plane packing distances between MNPs of the same charge remain low, surface coverage is often below 30 %, because of coulomb repulsion.

Most readily prepared charged gold NPs are citrate stabilized gold NPs in dilute aqueous solution but their application to the conventional LbL process is difficult because of their low stability. The electrostatic repulsion of citrate layers on the surface of gold NPs provides sufficient stability only at low concentration and ionic strength of the aqueous solution. However, Schmitt et al. successfully demonstrated their LbL deposition with the cationic polyelectrolyte poly(ally1 1-amine hydrochloride) to give surprisingly well ordered layers of MNPs [67]. The long term stability of these multilayer composite films remains questionable since citrate stabilized gold NPs likely coalesce over time in the given environment.

Abdelrahman et al. attempted to circumvent the problem of low stability by depositing layers of 1,4-benzenedimethanethiol in-between layers of citrate stabilized gold NPs [68, 69]. The thiols easily replace the citrate groups and generate a stable binding layer between each layer of gold NPs. Consequently, the process does not depend on electrostatic interactions but the formation of quasi covalent gold-sulfur bonds. However, the authors do observe growth of the gold NPs from 2.6 nm to 5–6 nm after the deposition despite the presence of dithiols. Clearly, the protection with citrate groups does not completely prevent coalescence of the gold NPs, which likely occurs before they are fully immobilized by the 1,4-benzenedimethanethiol linker molecules.

Bifunctional ligands with a thiol group at one end and a charged or chargeable group at the other end generate more stable charged MNPs. Hicks et al. reported the LbL deposition of hexanethiol/mercaptoundecanoic acid protected gold NPs with poly(allylamine hydrochloride) and hexanethiol/4-aminothiophenol protected gold NPs with poly(sodium 4-styrene sulfonate) [70]. They chose NPs with core

diameters of about 1.6 nm to match the thickness of each polymer layer but still observed multilayer deposition of gold NPs in one cycle, which they reasoned with entanglements between loose polymer chains and depositing gold NPs. Deposition kinetics were most drastically affected by changes in pH. This work was expanded by Song et al. who LbL deposited anionic gold NPs with a mixed monolayer of hexanethiol, ferrocenylhexanethiol, and mercaptoundecanoic acid alternating with poly(allyl 1-amine hydrochloride) [71]. Again, the adsorption density of the gold NPs in the multilayers greatly depended on pH and ionic strength of the polyelectrolyte solution. A pH of 5.8 was found to be optimal to ensure gold NPs and polyelectrolytes are sufficiently charged. Alternating LbL deposition of anionic hexanethiol/mercaptoundecanoic acid protected gold NPs with a cationic dendrimer instead of a polyelectrolyte also generated multilayers as demonstrated by Zhao et al. [72]. The methodology could be applied to gold NPs of smaller (3 nm) and larger (16 nm) core diameters and variations in ionic strength were used to alter interparticle distances.

Peter et al. attempted the LbL deposition of *N*,*N*,*N*-trimethyl-(11-mercaptoundecyl)ammonium chloride and mercaptoundecanoic acid protected gold NPs without the aid of polyelectrolytes or other mediating organic molecules [73]. Unfortunately, the oppositely charged gold NPs form clusters of sizes between 100 and 6000 MNPs instead of alternating monolayers. This result may not be particularly surprising considering the low density packing of the first layer of gold NPs on the substrate and the high affinity between oppositely charged MNPs. Cluster size distributions appeared to follow an exponentially decaying function, which may allow for a predictable nanostructuring of surfaces by this approach.

A more successful approach to the LbL deposition of oppositely charged MNPs was reported by Kawada et al. [74]. They coated silver NPs with polyethyleneimine and poly(sodium 4-styrenesulfonate) to give cationic and anionic MNPs of average diameters of 13.1 and 8.8 nm, respectively. Their alternating LbL deposition onto a supporting membrane of anodic aluminum oxide generated well-ordered layers of cationic and anionic MNPs that were tested as ultrafiltration membranes.

In general, protection of MNPs by polyelectrolytes generates more robust MNPs than a monolayer of protective organic ligands. For instance, gold NPs of a core diameter of 4.76 nm do not grow in size over a period of weeks if protected by poly (diallyldimethylammonium chloride) as confirmed by UV-vis spectroscopy [75]. LbL deposition of these gold NPs with an anionic polymer (s-119) produced stable multilayer films although the estimated layer thickness of 3.4 nm for each gold NP layer, determined by ellipsometry, is too small based on an overall NP diameter of >4.8 nm. This discrepancy may be reasoned with significant packing distances between gold NPs within each layer and interpenetrating layers.

Polymer coated MNPs may also be generated within a multilayer of cationic and anionic polyelectrolytes. A comparative study was provided by Rivero et al. who examined silver NPs capped with poly(acrylic acid, sodium salt) that were LbL deposited together with poly(allylamine hydrochloride) [76]. Alternating deposition of poly(acrylic acid) protected silver NPs with poly(allylamine hydrochloride) produced multilayers of distinct layer structure with progressive deposition of

MNPs, although the morphology of these multilayers may not be uniform. In contrast, silver NPs were formed only in the most outer layer when LbL deposited mulitlayers of poly(acrylic acid) and poly(allyl 1-amine hydrochloride) were first exposed to a solution of silver (I) ions and then to a solution of the reducing complex dimethylamine borane.

A major limitation of the use of charged MNPs for the formation of multilayer films by LbL deposition is the electrostatic repulsion between MNPs of the same charge because it causes a large spacing between MNPs and, consequently, a low surface coverage (<30 %). Cho and co-workers developed a methodology that incorporates initially hydrophobic MNPs into ionic or strongly polar multilayer films which they termed amphiphilic LbL assembly [77, 78]. They alternately deposit a poly(amidoamine) dendrimer or poly(ethylene imine) and silver or gold NPs protected by a hydrophobic, weakly binding ligand such as palmitic acid or tetraoctylammonium bromide. At the interface the hydrophobic ligands are partially replaced by the more strongly binding hydrophilic dendrimer or polymer and mostly replaced after the deposition of the next layer of hydrophilic dendrimer or polymer (Fig. 8.18). The group achieved in plane packing densities of MNPs up to 77 % and always above 50 %. If polyelectrolytes are used, such as poly(4-sodium, styrenesulfonic acid), the packing density of the initially hydrophobic MNPs could be increased by up to 20 % by an increase in ionic strength. For example, increase

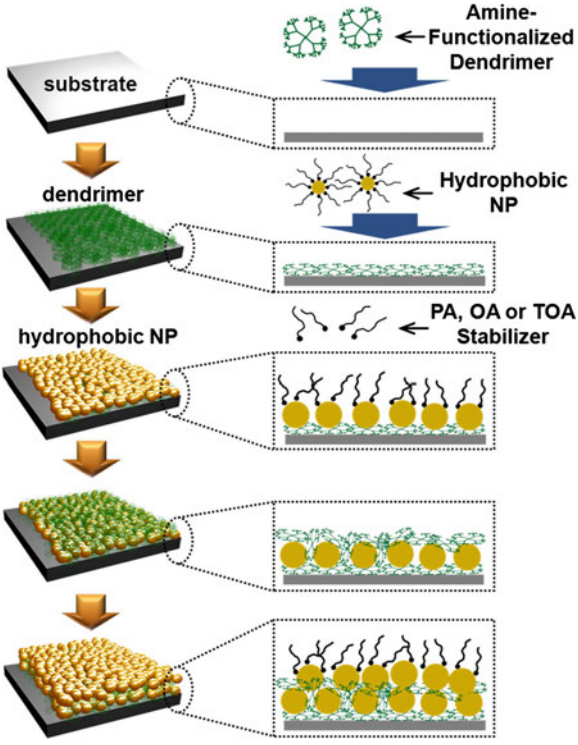

Fig. 8.18 Schematic diagram showing the preparation of $(dendrimer)_n$ multilayer films by LbL assembly of hydrophobic MNPs and hydrophilic dendrimer in organic media. Reprinted (adapted) with permission from [77]. Copyright 2013 American Chemical Society

of the concentration of NaCl in the coating solution increased the amount of deposited MNPs and poly(4-sodium, styrenesulfonic acid) until a concentration of 0.2 M was reached. The authors also demonstrated the general applicability of this procedure by processing other NPs such as metal oxides Fe_3O_4, TiO_2, and MnO.

8.3.3 LbL Deposition of Neutral MNPs Based on H- and Covalent Bonds as Well as Other Non-ionic Interactions

LbL deposition is also possible with non-ionic dendrimers based on poly(amido-amine) or poly(propylene imine) if functionalized with exo-amino groups for better attachment to gold NPs [79]. Dendrimers that attach to gold NPs with multiple amine groups were found to even replace alkanethiol ligands that individually bind stronger to the gold surface but the authors used dodecylamine protected gold NPs in this study. The conformational flexibility of these dendrimers also allows them to closer pack to the metal surface and more effectively fill spaces between MNPs. Binding between different layers is mainly facilitated by H-bonding between amine groups not involved in the binding to the gold surface and by van der Waals interactions. The overall morphology of these films is porous grainy due to deposition of spherical dendrimers with spherical MNPs.

Finally, LbL deposition may be achieved by covalently linking MNPs via bifunctional linker molecules or chemical reactions between two functional groups. Bifunctional linkers that have been applied to link NPs together contain thiol, amine, siloxane, alcohol, and isocyanide functional groups [80–82]. An early work by Brust et al. demonstrated the use of nonane-1,9-dithiol to LbL assemble gold NPs and CdSe particles [83]. Musick et al. used 2-mercaptoethanol as cross-linker between gold NPs to generate multilayer films but the morphology of the films is porous and no close-packing of gold NPs is observed [80].

However, 2-mercaptoethanol as spacer does not provide sufficient distance between gold NPs and coalescence of the gold cores is observed over time. A study by Supriya et al. demonstrates how the thermal stability of cross-linked gold NP films increases with increasing spacer length by comparing 2-mercaptoethanol, 1,6-hexanedithiol, and 1,10-decanedithiol [84]. In this study, coalescence of gold NPs was desired because conductive pathways are generated and was promoted by heat treatments at different temperatures and for different periods of time. The initial resistance of the films, for example, increased from 50 Ω to 1 MΩ and to >100 MΩ with increasing spacer length of the three different linker molecules.

Instead of using linker molecules with two terminal linking groups it is also possible to generate new chemical bonds between two protective ligands. An interesting example is the preparation of gold NPs that are coated with *O*-carboxymethyl chitosan and cross-linked in the multilayer by exposure to glutaraldehyde [85]. The chitosan polymer is assumed to coordinate to the gold NPs

predominantly through their carboxylic acid groups, which leaves the amine groups available for reactions with the dialdehyde cross-linker to generate diimines. Li et al. chose a different approach by LbL depositing polyphenylene dendrimer-stabilized gold nanoparticles with alkynes in their peripheries with a functional polymer that contains peripheral azide groups for "click" chemistry [86].

8.4 Self-organizing Metal Nanoparticles

Self-organization probably is the most powerful method at hands for the controlled three-dimensional nano-structuring of materials over macroscopic length scales, which is mainly aided by the cooperative behaviour between individual self-organizing units (usually molecules). Self-organization also is the central process underlying successful technologies such as liquid crystal displays. It is an intrinsically three-dimensional process, similar to crystallization, but can generate structures of various degrees of order and mobility. Equally important for its remarkable ability to nano-structure materials and to its technological success, however, its cooperative response to relatively weak external directional forces, such as electric and magnetic fields and surface alignment layers, that generate domains of uniform orientation and structure over centimeter length scales [87].

Phases formed by self-organizing compounds are named mesophases because their degree of order is in-between that of an isotropic liquid and a single crystal. Mesophases, by definition, are thermodynamically stable and mostly anisotropic phases, in contrast to kinetically trapped phases of similar structures. Bulk materials form mesophases by change of temperature (thermotropic mesophases) whereas the mesomorphism of solutions (lyotropic mesophases) depends on concentration and temperature. Thermotropic mesophases are subdivided based on their molecular (shape anisotropy) and supramolecular structures. Rod-shaped (calamitic) molecules form nematic phases, which display solely orientational order, and smectic phases that display orientational and one-dimensional positional order. However, smectic phases with higher positional order are also known. Disc-shaped (discotic) and wedge-shaped molecules preferentially self-organize into columnar mesophases of orientational and two-dimensional positional order but nematic phases with just orientational order have also been observed (discotic nematic), although they remain rare. Spherical and cone-shaped molecules usually arrange into cubic structures that are characterized by positional order and a lack of orientational order.

Early designs of compounds that self-organize into mesophases were mainly based on the shape anisotropy of rod-like molecules, which is sufficient for the introduction of anisotropy due to orientational order (nematic mesophases). Subsequently, microphase segregation and directed molecular interactions were added as design tools that gave access to layered (smectic) mesophases of rod-shaped molecules that may display positional order from one-dimension to quasi three-dimensions. After about 90 years of research on rod-shaped mesogens, disc-shaped structures were added to the tool kit in the 1970s as a new type of shape-

anisotropy. Concepts of self-organization and mesomorphism have seen a significant extension well beyond the classical structural motifs described above over the past 20 years. Judicious application of shape anisotropy, microphase segregation, directed molecular interactions, and self-assembly has converted molecules with low or unfavorable aspect ratios, including ionic molecules, into compounds that display mesophases over a wide range of temperatures. These new developments made it conceivable to convert quasi spherical nanoparticles into self-organizing structures, similar to what has been demonstrated for C_{60} [88, 89].

Most of the reported work on self-organizing MNPs has been concerned with gold NPs, although the first studies on self-organizing MNPs involved metal oxide NPs. A rather comprehensive review of all reported self-organizing MNPs was provided by Nealon et al. [90] while a more general overview of NPs in self-organizing materials was provided by Bisoyi and Kumar [91]. The following part will be mainly concerned with MNPs that self-organize into thermotropic mesophases but we note that micellar [92] and lyotropic [93] NPs have also been reported. Similarly, self-organizing materials that are generated by doping NPs into self-organizing compounds, usually liquid crystals, are not covered here [94, 95]. Finally, self-organizing rod-shaped and other metal nanoparticles of anisotropic shape are omitted because they have been discussed in the previous chapter.

The prominent role of gold NPs for the synthesis of self-organizing MNPs is easily explained by their well established and versatile coating with monolayers of organic molecules, mostly thiolates, and the relatively straightforward synthesis of gold NPs with small diameters between 1 and 5 nm [96]. They are either prepared directly in the presence of the final organic thiolate ligand (e.g. modified Brust–Schiffrin procedure [97, 98]) or by a two-step procedure in which the gold NPs are first synthesized in the presence of a weaker binding ligand (e.g. alkyl amine or thiolate with shorter alkyl chain) that is subsequently fully or partially exchanged by a stronger binding desired ligand via a solvent-mediated ligand exchange process [99]. Gold NPs prepared with weaker binding ligands usually display smaller size distributions but a complete removal of this ligand by exchange processes is often difficult. However, the presence of two different ligands appears to be advantages to the self-organization properties of MNPs because they can change the overall shape of MNPs and their interparticle interactions [100]. A similar response was observed for MNPs at interphases, e.g. when processed by the LB method, as described earlier in this chapter [37].

Regardless of the applied synthesis method, purification of the MNPs is a crucial and difficult step because of their high surface area and often overall amphiphilic character (charged metal surface partially covered with a monolayer of hydrophobic alkylthiolate ligands). Depending on the exact reaction conditions, excess of organic ligands, surfactant molecules, and side-products from the applied reducing agent must be removed, which is usually achieved by repetitive precipitation. However, particle sizes often increase with every precipitation step due to coalescence, which is an indication of the dynamic binding of thiolate ligands to gold NP surfaces and the incremental removal of soluble ligands with every precipitation step [17, 101]. Gold NPs with rather strongly bond thiolate ligands may also be

purified by gel-permeation chromatography [102]. Product purity and ligand ratios are usually determined by a combination of solution nuclear magnetic resonance (NMR) spectroscopy, thermal analysis (Differential scanning calorimetry (DSC) and thermogravimetric analysis (TGA)), elemental analysis, and TEM [103–105].

Mesomorphism of MNPs is investigated by three main methods, variable temperature polarized optical microscopy (POM), DSC, and variable temperature powder XRD. Most important for a structural analysis of mesophases of MNPs is powder XRD, ideally of aligned domains of the mesophases, although their interpretation may be complex because MNPs may adapt their shapes to the optimize packing within the geometrical restrictions of the displayed phase. The relatively small number of reflections makes an analytical solution of the XRD pattern impractical. Probably the most reliable approach to the analysis of these diffraction patterns is the comparison of simulated diffractions patterns based on calculated density distributions within simulated packing structures, which has been widely applied by Ungar and others.

Investigation of the mesomorphism of monolayer protected gold NPs is complicated mainly by the dynamic character of the organic layer, when compared to the self-organization of molecular structures. Thiolate ligands relatively easily move on the surface of gold NPs and also reversibly desorb and adsorb, especially at elevated temperatures [106, 107]. Consequently, the average diameter of the gold core may increase with time at temperatures above 100–150 °C due to coalescence of gold cores. Perhaps even more important is that the distribution of organic ligands on the surface of gold NPs changes depending on the environment. This can benefit the mesomorphism by rendering an isotorpic spherical structure to an anisotropic prolate spheroid (increase in shape anisotropy) [108] and similar structural changes of MNPs due to ligand mobility have been observed at interfaces as reported earlier in this chapter in the part on LB films [51].

The quasi spherical shape of MNPs with truncated octahedral or related metal structures would make them prime candidates for the formation of cubic mesophases but those are rarely observed in these materials. In fact, attachment of organic ligands that have no mesogenic structure, such as a simple alkylthiolates, has not generated self-organizing MNPs. A perhaps obvious remedy is the attachment of ligands that self-organize themselves (mesomorphic ligands) or have typical features of self-organizing compounds (mesogenic). This approach has broadly been applied not only to the conversion of MNPs into self-organizing compounds but also to generate MNPs that can be easily doped into liquid crystalline host materials [109]. Most of the attached mesomorphic and mesogenic ligands contain rod-shaped rigid structures and will be discussed first, while relatively few examples exist on ligands with disc-shaped rigid structures.

Although the number of self-organizing gold NPs is still limited, some general design criteria may be cautiously extracted from the studies that have been reported [90, 91]. All mesomorphic and mesogenic ligands that have been investigated have a flexible spacer between the rigid part and the linking group (usually thiolate) to the gold NP surface. Both length and structure of the spacer chain must ensure sufficient mobility for the rigid part to arrange (self-organize) into the most

favourable packing structure. A good source of guidance for the prediction of optimal spacer chains may be the large volume of work on liquid crystalline side-chain polymers. For most of the reported self-organizing MNPs the overall length of ligands is commensurate with the diameter of the MNP core, which limits the required size of the metal core to values well below 10 nm unless unusually large organic ligands are available. An increase in length (packing volume) of mesogenic ligands with regard to the metal core likely aids mesomorphism but may be synthetically challenging, while a significant decrease in length (packing volume) may not only compromise mesomorphism but also the stability of the MNPs. In addition to the average size of MNPs their size distribution also appears to be crucial. Experimental and theoretical studies suggest that an increase in size distribution diminishes the propensity for self-organization, similar to what has been observed for the self-assembly of MNPs.

8.4.1 LC MNPs with One Type of Ligand

Mesomorphic MNPs were first reported in 2001 by coating gold NPs with calamitic liquid crystals through thiolate linking groups. The rigid part of the ligands consisted of a (cyclohexyl)phenoxy group (Fig. 8.20) that provided sufficient shape anisotropy and microphase segregation for the formation of nematic and smectic mesophases. Attachment of these ligands to gold NPs of 3 nm core diameter generated mesomorphic MNPs that display mesophases at a wider temperature range than the free ligands but, unfortunately, the mesophase(s) were not investigated by XRD and their structure(s) remained unassigned [110] (Fig. 8.19).

Four years later a similar approach was reported that employed mesomorphic ligands with cyanobiphenyl as rigid parts (Fig. 8.20) [112]. Both, TEM and XRD data for the sample with dodecyl spacer chains and a gold core of 2.7 ± 0.5 nm diameter revealed a string-like arrangement of gold NPs in their mesophase with distances between strings of about 6 nm, an interparticle distance within each string of 2–3 nm, and an overall length of each string between 13 and 60 nm. These results provided the first evidence for an uneven distribution of mesomorphic ligands on the surface of gold NPs in an anisotropic mesophase. The observed distances agree with a packing model shown in Fig. 8.21 that proposes a preferential alignment of the ligands in-between strings to generate a likely partially interdigitated antiparallel double layer of cyanobiphenyl groups. However, the obtained data were still insufficient for an assignment of the type of mesophases but it likely is a nematic mesophases. The temperature range of 110–130 °C is significantly wider and higher in temperature than the free ligand, which forms a monotropic nematic mesophases between 75.9 and 71.7 °C. Corresponding gold NPs with shorter spacer chains given in Fig. 8.19 were studied much later and in more detail. The refined structural interpretation of the new data overall corroborated the initially proposed packing structures [108].

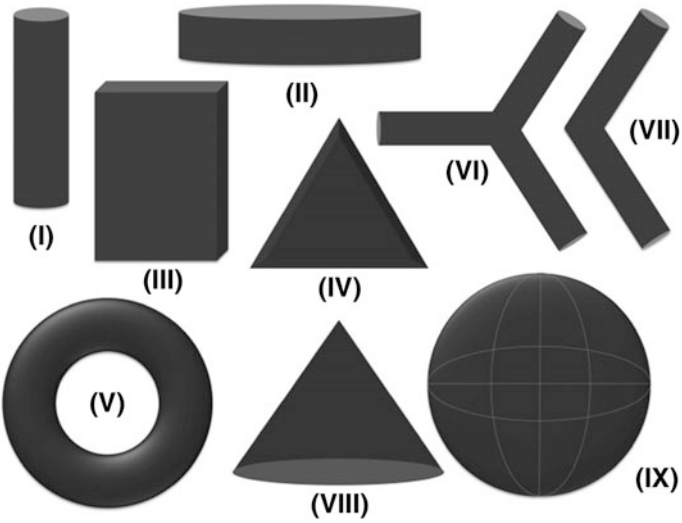

Fig. 8.19 Cartoons of shapes of molecular cores that have been successfully converted into liquid crystals: *I* calamitic; *II* discotic, *III* board-shaped, *IV* wedge-shaped, *V* ring-shaped, *VI* star-like, *VII* bent-rod, *VIII* conical, and *IX* spherical motifs. Reprinted from [111], with permission from Elsevier

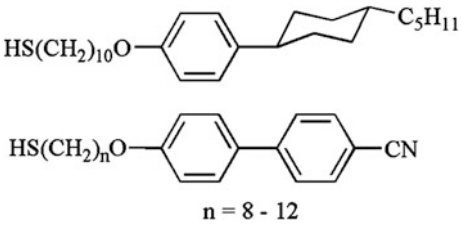

Fig. 8.20 Mesomorphic thiol ligands based on (cyclohexyl)phenoxy [110] and cyanobiphenyl rigid [112] parts that were used in early studies of mesomorphic gold NPs

However, the authors of the latter study presented a more sophisticated and general model that has been commonly accepted and applied in packing models for nematic, lamellar, and columnar mesophases (Fig. 8.22). They proposed the formation of hard pole areas with strong interactions between ligands and much less densely packed equator areas that results in a distortion from isotropic spheroidal to anisotropic prolate spheroidal structure. The described structural changes of the ligands are mainly based on conformational changes and require a relatively low density packing of ligands to provide sufficient space for these changes. Rearrangements of ligands, although possible, are likely not involved in this distortion of the ligand shell. MNPs that pack in local rectangular or hexagonal

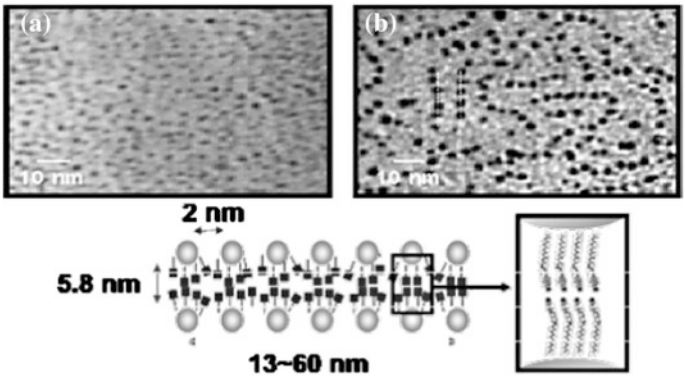

Fig. 8.21 TEM images of Au@6_{12} **a** before and **b** after thermal treatment. *Below* Proposed model of the nanoparticle arrangement within the strings. Reproduced by permission of The Royal Society of Chemistry. Shown to the right is a simplified illustration of a local rectangular arrangement of gold NPs in a mesophase. Reprinted with permission from [90]. Copyright 2012 Beilstein Institute

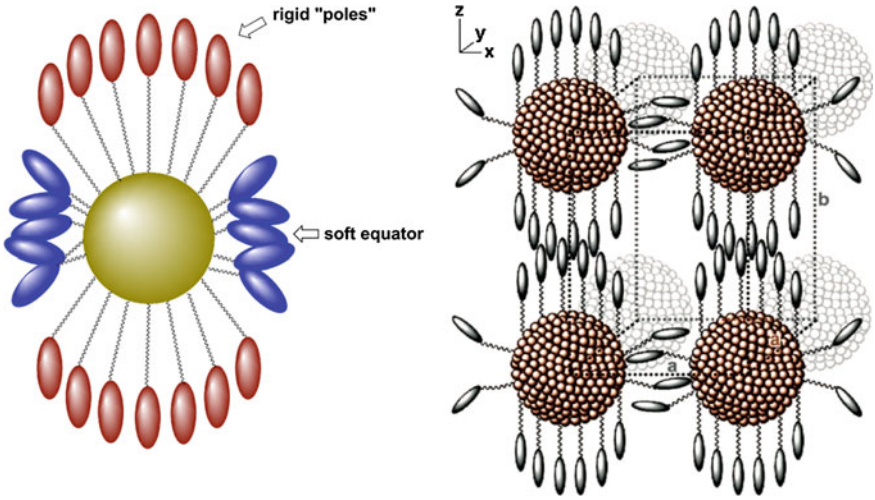

Fig. 8.22 Generation of rigid "poles" and soft equator areas by ligand deformation at the surface of gold NPs (*left*). Simplified illustration of a local rectangular arrangement of deformed gold NPs in a mesophase (*right*). Reprinted with permission from [90]. Copyright 2012 Beilstein Institute

structures display local A_2 order between the poles and local A_d order between the equators. These different environments may also explain why the observed XRD data suggest the coexistence of more than one packing structure.

8.4.2 LC MNPs with Two or More Types of Ligands

Overall, the attachment of just mesomorphic ligands appears to have serious limitations because attempts to generate mesomorphic gold NPs with more densely packing dendritic ligands and laterally attached rod-like ligands failed [113]. Much more versatile is the use of mixed ligands that is typically achieved by incomplete ligand exchange reactions of thiol ligands by other thiol ligands. Several comprehensive studies with alkylthiols as primary ligands that were partially exchanged by much larger mesomorphic ligands have been conducted by Mehl and Ungar and co-workers [114–116] and Gorecka and co-workers [117, 118]. It became apparent in all these studies that the ligands are not distributed evenly but the mesomorphic ligands form domains at the poles and the alkylthiols form domains at the equator to generate prolate spheroidal or even cylindrical shapes. In contrast to the previous examples of prolate spheroidal structures the mechanism is different here as it relies on the migration of ligands rather than conformational changes.

In addition to the application of mixed ligand layers both groups also employed more sophisticated mesomorphic ligands that display a range of nematic and smectic mesophases. Examples of ligands with terminal connections that were used by Gorecka and co-workers are given in Fig. 8.23. Typical ratios between primary alkylthiol ligands and mesomorphic ligands in molar ratios were 1:1–2:1 based on NMR studies but changes in ratios within this range had only minor effects on the mesomorphism. Variation of the chain lengths of the alkylthiols, on the other hand, had profound effects on the mesomorphism. For example, the increase from hexyl to octyl to dodecyl thiols changed the packing structures of the cylindrically shaped MNPs from smectic to modulated smectic to columnar as illustrated in Fig. 8.24. We note, however, that the organic domains in all of these materials appear to be in an amorphous state rather than any orientationally and/or positionally ordered state, which is consistent with the observed low birefringence.

The incorporation of ligands with two rigid parts (dimeric) was investigated in a recent publication by Gorecka and co-workers [119]. A comparison of the "dimeric ligands" with conventional "monomeric" ligands revealed distinct structural

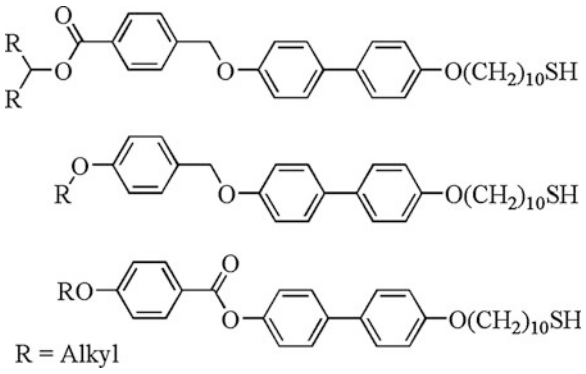

Fig. 8.23 Mesomorphic ligands for gold MNPs that display smectic and nematic polymorphism [117, 118]

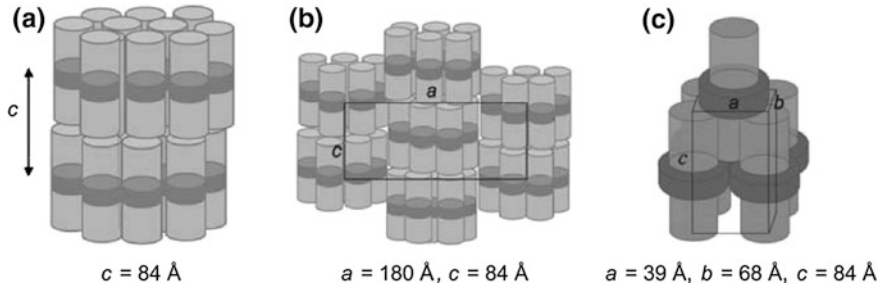

Fig. 8.24 Proposed structural models resulting from ligand migration at the NP surface: **a** smectic for hexyl thiol as primary ligand **b** modulated smectic for octyl thiol as primary ligand **c** columnar for dodecyl thiol as primary ligand, respectively. *Light grey* and *dark grey* indicate the disposition and form of the mesogenic groups and alkylthiols respectively. Reprinted with permission from [118]. Copyright 2010 Wiley-VCH Publishers

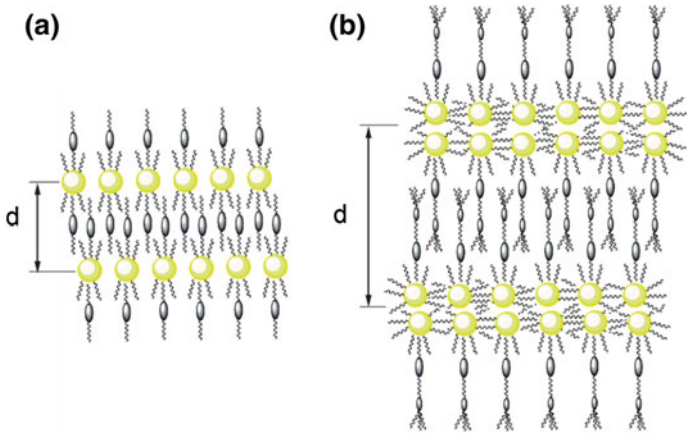

Fig. 8.25 Schematic drawing of the arrangement of the hybrid particles in a smectic phase for materials with **a** monomeric ligands (series AuL1) and **b** dimeric secondary ligands (series AuL2 and AuL3). For clarity of the picture only a limited number of molecules grafting the metallic clusters are shown. Reproduced from [119] with permission of The Royal Society of Chemistry

differences, most notably the formation of a bilayer of gold NPs in-between the organic layers of smectic mesophases (Fig. 8.25). Also important is the observation of orientational order in the organic layer that generates measurable birefringence. Another recent study clearly reveals the importance of the flexible spacer between the mesogenic unit and the MNP [7]. Longer spacers not only promote mesomorphism by lowering the melting temperatures of the MNPs but also affect what types of self-organized structures are formed. Observed here is the change from a 1D (lamellar) structure to 3D superlattices with base-centered

orthorhombic unit cells. Interestingly, the length of the alkylthiol has no effect on the formed structure.

Lateral attachment of mesomorphic ligands has been successfully demonstrated by Mehl and co-workers [114–116] and generates cylindrical MNP structures that preferentially arrange into columnar stacks. This seems to be a more general preference as it was also observed for related silsesquioxanes [120]. The rigid parts of the mesomorphic ligands are aligned parallel to the columnar stacks but the packing volume (length) of the alkylthiol ligands influences whether the columns are modulate or not. The former arrange into a rhombohedral phase whereas the latter arranges into a hexagonal phase (Fig. 8.26). Optical textures of these columnar mesophases are characteristic of a nematic phase, which implies the absence of longer range positional order.

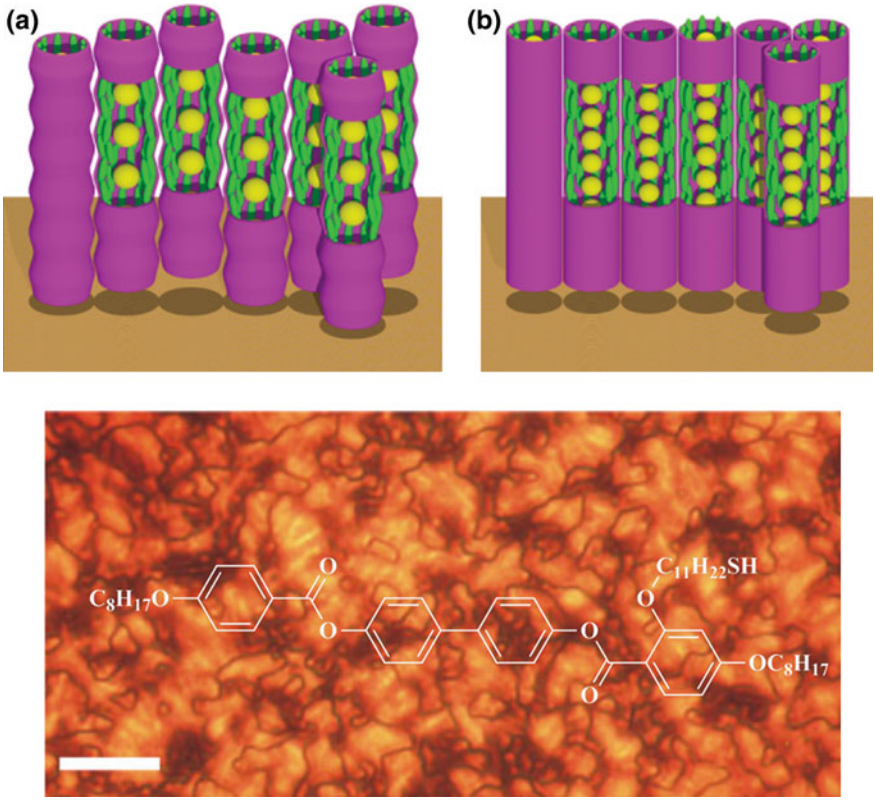

Fig. 8.26 Schematic models of the gold string structures (*top*). **a** Rhombohedral phase of gold NPs with dodecyl thiol as primary ligand and **b** hexagonal columnar phase of gold NPs with hexyl thiol as primary ligand; *yellow* gold nanoparticles, *green* mesogens. Threaded nematic texture of the MNP with dodecyl thiol as primary ligand and the shown mesogen as secondary ligand as observed by polarized optical microscopy at room temperature (*bottom*). Reprinted with permission from [114]. Copyright 2009 Wiley-VCH Publishers

Lateral attachment of bent-rod mesomorphic ligands has not generated any mesomorphic MNPs, which is often reasoned with the high melting temperatures of these ligands. Thiol desorption and subsequent growth of the MNPs occurs before the ligands actually melt into a more fluid phase [117, 121]. Dendritic and structural related ligands have been attached to gold NPs in an attempt to better fill the space around MNPs and to increase the volume fraction of the organic layer. Especially an increase of the volume fraction of the deformable and shape-directing organic layer should enhance the mesomorphic properties. This can be achieved by increasing the size of the ligands or decreasing the size of the gold cores. However, typical core diameters of the reported mesomorphic gold NPs are between 1 and 3 nm, which does not leave much room for a further decrease in core size.

Dendritic ligands have converted many different types of cores into mesomorphic compounds [122] but the first attempts of generating mesomorphic MNPs were unsuccessful [113], even though highly ordered arrangements of these MNPs on carbon-coated copper grids were observed. These findings were reasoned with the tight packing of the dendritic ligands that does not allow for distortions of the overall shape of the MNP by conformational changes and ligand migration. The first successful design employed dendrons that were attached to the MNP via a flexible spacer and, consequently, was conformationally more flexible [123]. These MNPs displayed cubic and 2-dimensional hexagonal mesophases. This report was followed by only one other successful attempt with MNPs [124] but several mesomorphic metal oxide NPs with dendritic ligands have been reported [125–127].

Finally, the attachment of discotic mesomorphic ligands to MNPs has not yet produced mesomorphic MNPs as neat material but drastically enhanced their ability to be doped into columnar mesophases of discotic liquid crystals of similar structures [128, 129]. However, only very few examples have yet been studied and it is likely that mesomorphic MNPs with discotic ligands will be successfully prepared in the near future.

Clearly, the development of self-organizing MNPs is still in its infant state and mainly concerned with structure property relations. Very few reports have been concerned with the properties of the obtained materials but, in principle, they should be similar to the interesting properties that have been reported for self-assembled MNPs. A recent publication, for example, reports the anisotropic plasmonic properties of silver and gold NPs in their lamellar mesophases [130].

8.5 Conclusions and Outlook

The ability to control packing structures and distances of metal nanoparticles (MNPs) in monolayers and multilayers is fundamental for many applications such as sensorics, catalysis, electronic devices, optical devices, spectroscopy, and membranes. Processing MNPs by the Langmuir-Blodgett technique has been particularly successful for the generation of two-dimensional hexagonal close-packed

monolayers of MNPs with tunable interparticle spacing. Although above examples exemplify the verge of fabricating highly-ordered, defect-free LB films, defects in the monolayers remain as an obstacle mainly due to polydisperse sizes and self-aggregation of nanoparticles. Enhanced LB properties are obtained with amphiphilic NPs such as Janus-type MNPs, which may produce highly-ordered LB films. The stability of these films may be improved by the use of multidentate ligands or by cross-linking deposited MNPs with ligands that contain two terminal linking groups.

Only few examples of LB multilayer films have been reported, which reflects the difficulty of controlling multiple depositions of ordered monolayers. Layer-by-Layer (LbL) deposition is more commonly applied to the fabrication of multilayer films that contain MNPs. Most of the early examples of LbL deposition relied on ionic MNPs but surface coverages of larger than 30 % are difficult to achieve because of coulomb repulsion between equally charged MNPs. Much higher packing densities of >75 % were achieved with neutral, hydrophobic MNPs and new processing techniques in non-polar solvents provide new options for the preparation of more ordered and stable LbL deposited monolayers.

Lastly, self-organizing MNPs give access to a range of different three-dimensionally ordered structures such as lamellar (smectic), columnar, and cubic arrangements of MNPs. The predominant design relies on the attachment of liquid crystalline ligand molecules via long flexible spacers. In fact, the length of the flexible spacer is critical as the formation of liquid crystal phases requires the conformational rearrangement of the ligands to generate overall more elongated NPs. Alternatively, the shape of MNPs containing a mixture of at least two ligands may change due to domain formation of specific ligands.

A major limitation is still the synthetic availability of monodisperse, compositionally defined, and stable MNPs. Especially LB-studies and self-organization of MNPs are strongly affected by impurities, such as excess of protective ligand, and polydispersity of their size, shape, and composition. Consequently, new synthetic strategies and designs that generate stable, monodisperse, and purer MNPs with the desired chemical functionality are at the heart of any advancement in this area of research.

References

1. M. Grzelczak, J. Vermant, E.M. Furst, L.M. Liz-Marzán, Directed self-assembly of nanoparticles. ACS Nano **4**, 3591–3605 (2010)
2. A. Boker, J. He, T. Emrick, T.P. Russell, Self-assembly of nanoparticles at interfaces. Soft Matter **3**, 1231–1248 (2007)
3. S. Kinge, M. Crego-Calama, D.N. Reinhoudt, Self-assembling nanoparticles at surfaces and interfaces. ChemPhysChem **9**, 20–42 (2008)
4. Z. Nie, A. Petukhova, E. Kumacheva, Properties and emerging applications of self-assembled structures made from inorganic nanoparticles. Nat. Nanotechnol. **5**, 15–25 (2010)

5. A. Klinkova, R.M. Choueiri, E. Kumacheva, Self-assembled plasmonic nanostructures. Chem. Soc. Rev. **43**, 3976–3991 (2014)
6. K. Ariga, Q. Ji, J.P. Hill, Y. Bando, M. Aono, Forming nanomaterials as layered functional structures toward materials nanoarchitectonics. NPG Asia Mater. **4**, 17 (2012)
7. W. Lewandowski, K. Jatczak, D. Pociecha, J. Mieczkowski, Control of gold nanoparticle superlattice properties via mesogenic ligand architecture. Langmuir **29**, 3404–3410 (2013)
8. X.G. Peng, Y. Zhang, J. Yang, B.S. Zou, L.Z. Xiao, T.J. Li, Formation of nanoparticulate Fe_2O_3-stearate multilayer through the Langmuir-Blodgett method. J. Phys. Chem. **96**, 3412–3415 (1992)
9. M. Sastry, K.S. Mayya, V. Patil, Facile surface modification of colloidal particles using bilayer surfactant assemblies: a new strategy for electrostatic complexation in Langmuir-Blodgett films. Langmuir **14**, 5921–5928 (1998)
10. K. Gmucova, M. Weis, V. Nadazdy, E. Majkova, Orientation ordering of nanoparticle Ag/Co cores controlled by electric and magnetic fields. ChemPhysChem **9**, 1036–1039 (2008)
11. H. Watanabe, M. Nishimura, Y. Fukui, K. Fujimoto, Development of a particle nanoimprinting technique by core-shell particles. Langmuir **30**, 1630–1635 (2014)
12. Y.C. Tian, J.H. Fendler, Langmuir-Blodgett film formation from fluorescence-activated, surfactant-capped, size-selected CdS nanoparticles spread on water surfaces. Chem. Mater. **8**, 969–974 (1996)
13. S.A. Iakovenko, A.S. Trifonov, M. Giersig, A. Mamedov, D.K. Nagesha, V.V. Hanin, E.C. Soldatov, N.A. Kotov, One- and two-dimensional arrays of magnetic nanoparticles by the Langmuir-Blodgett technique. Adv. Mater. **11**, 388–392 (1999)
14. A.R. Tao, J. Huang, P. Yang, Langmuir-Blodgettry of nanocrystals and nanowires. Acc. Chem. Res. **41**, 1662–1673 (2008)
15. K. Kolasinski, *Surface Science: Foundations of Catalysis and Nanoscience* (Wiley, 2002)
16. A.R. Tao, Nanocrystal assembly for bottom-up plasmonic materials and surface-enhanced Raman spectroscopy (SERS) sensing. Pure Appl. Chem. **81**, 61–71 (2009)
17. J.C. Love, L.A. Estroff, J.K. Kriebel, R.G. Nuzzo, G.M. Whitesides, Self-assembled monolayers of thiolates on metals as a form of nanotechnology. Chem. Rev. **105**, 1103–1169 (2005)
18. J.H. Fendler, Self-assembled nanostructured materials. Chem. Mater. **8**, 1616–1624 (1996)
19. E. Pohjalainen, M. Pohjakallio, C. Johans, K. Kontturi, J.V.I. Timonen, O. Ikkala, R.H.A. Ras, T. Viitala, M.T. Heino, E.T. Seppala, Cobalt nanoparticle Langmuir-Schaefer films on ethylene glycol subphase. Langmuir **26**, 13937–13943 (2010)
20. R.K. Gupta, K.A. Suresh, S. Kumar, Monolayer of amphiphilic functionalized gold nanoparticles at an air-water interface. Phys. Rev. E **78**, 032601 (2008)
21. A. Perro, S. Reculusa, S. Ravaine, E. Bourgeat-Lami, E. Duguet, Design and synthesis of Janus micro-and nanoparticles. J. Mater. Chem. **15**, 3745–3760 (2005)
22. H. Zhang, Y. Liu, D. Yao, B. Yang, Hybridization of inorganic nanoparticles and polymers to create regular and reversible self-assembly architectures. Chem. Soc. Rev. **41**, 6066–6088 (2012)
23. A. Swami, A. Kumar, P.R. Selvakannan, S. Mandal, M. Sastry, Langmuir-Blodgett films of laurylamine-modified hydrophobic gold nanoparticles organized at the air-water interface. J. Colloid Interface Sci. **260**, 367–373 (2003)
24. V. Aleksandrovic, D. Greshnykh, I. Randjelovic, A. Froemsdorf, A. Kornowski, S.V. Roth, C. Klinke, H. Weller, Preparation and electrical properties of cobalt-platinum nanoparticle monolayers deposited by the Langmuir-Blodgett technique. ACS Nano **2**, 1123–1130 (2008)
25. J.Y. Kim, S. Raja, F. Stellacci, Evolution of langmuir film of nanoparticles through successive compression cycles. small **7**(17), 2526–2532 (2011)
26. H. Song, F. Kim, S. Connor, G.A. Somorjai, P.D. Yang, Pt nanocrystals: shape control and Langmuir-Blodgett monolayer formation. J. Phys. Chem. B **109**, 188–193 (2005)
27. M.A. Mahmoud, M.A. El-Sayed, Comparative study of the assemblies and the resulting plasmon fields of Langmuir-Blodgett assembled monolayers of silver nanocubes and gold nanocages. J. Phys. Chem. C **112**, 14618–14625 (2008)

28. P.J.G. Goulet, D.S. dos Santos, R.A. Alvarez-Puebla, O.N. Oliveira, R.F. Aroca, Surface-enhanced Raman scattering on dendrimer/metallic nanoparticle layer-by-layer film substrates. Langmuir **21**, 5576–5581 (2005)
29. P.J.G. Goulet, N.P.W. Pieczonka, R.F. Aroca, Mapping single-molecule SERRS from Langmuir-Blodgett monolayers, on nanostructured silver island films. J. Raman Spectrosc. **36**, 574–580 (2005)
30. Y. Lu, G.L. Liu, L.P. Lee, High-density silver nanoparticle film with temperature-controllable interparticle spacing for a tunable surface enhanced Raman scattering substrate. Nano Lett. **5**, 5–9 (2005)
31. M.A. Mahmoud, C.E. Tabor, M.A. El-Sayed, Surface-enhanced Raman scattering enhancement by aggregated silver nanocube monolayers assembled by the Langmuir-Blodgett technique at different surface pressures. J. Phys. Chem. C **113**, 5493–5501 (2009)
32. X. Chen, X. Yang, W. Fu, M. Xu, H. Chen, Enhanced performance of polymer solar cells with a monolayer of assembled gold nanoparticle films fabricated by Langmuir-Blodgett technique. Mater. Sci. Eng., B **178**, 53–59 (2013)
33. J.Z. James, D. Lucas, C.P. Koshland, Gold nanoparticle films as sensitive and reusable elemental mercury sensors. Environ. Sci. Technol. Lett. **46**, 9557–9562 (2012)
34. C. Medina-Plaza, C. Garcia-Cabezon, C. Garcia-Hernandez, C. Bramorski, Y. Blanco-Val, F. Martin-Pedrosa, T. Kawai, J.A. de Saja, M.L. Rodriguez-Mendez, Analysis of organic acids and phenols of interest in the wine industry using Langmuir-Blodgett films based on functionalized nanoparticles. Anal. Chim. Acta **853**, 572–578 (2015)
35. J.Y. Park, Y. Zhang, M. Grass, T. Zhang, G.A. Somorjai, Tuning of catalytic CO oxidation by changing composition of Rh-Pt bimetallic nanoparticles. Nano Lett. **8**, 673–677 (2008)
36. Y.W. Zhang, M.E. Grass, W.Y. Huang, G.A. Somorjai, Seedless polyol synthesis and CO oxidation activity of monodisperse (111)- and (100)-oriented rhodium nanocrystals in sub-10 nm sizes. Langmuir **26**, 16463–16468 (2010)
37. K. Nørgaard, M.J. Weygand, K. Kjaer, M. Brust, T. Bjørnholm, Adaptive chemistry of bifunctional gold nanoparticles at the air/water interface. A synchrotron X-ray study of giant amphiphiles. Faraday Discuss. **125**, 221 (2004)
38. K.D. Comeau, M.V. Meli, Effect of alkanethiol chain length on gold nanoparticle monolayers at the air-water interface. Langmuir **28**, 377–381 (2012)
39. T. Matsumoto, P. Nickut, T. Sawada, H. Tsunoyama, K. Watanabe, T. Tsukuda, K. Al-Shamery, Y. Matsumoto, Deposition and fabrication of alkanethiolate gold nanocluster films on TiO_2(110) and the effects of plasma etching. Surf. Sci. **601**, 5121–5126 (2007)
40. J.R. Heath, C.M. Knobler, D.V. Leff, Pressure/temperature phase diagrams and superlattices of organically functionalized metal nanocrystal monolayers: the influence of particle size, size distribution, and surface passivant. J. Phys. Chem. B **101**, 189–197 (1997)
41. B.P. Gagnon, M.V. Meli, Effects on the self-assembly of n-alkane/gold nanoparticle mixtures spread at the air-water interface. Langmuir **30**, 179–185 (2014)
42. T.A. Sanders II, M.N. Sauced, J.A. Dahl, Langmuir isotherms of flexible, covalently crosslinked gold nanoparticle networks: increased collapse pressures of membrane-like structures. Mater. Lett. **120**, 159–162 (2014)
43. C.Y. Lau, H. Duan, F. Wang, C.B. He, H.Y. Low, J.K.W. Yang, Enhanced ordering in gold nanoparticles self-assembly through excess free ligands. Langmuir **27**, 3355–3360 (2011)
44. S.J. Lee, S.W. Han, H.J. Choi, K. Kim, Phase behavior of organic-inorganic crystal—temperature-dependent diffuse reflectance infrared spectroscopy of silver stearate. Eur. Phys. J. D **16**, 293–296 (2001)
45. H. Perez, R.M.L. de Sousa, J.P. Pradeau, P.A. Albouy, Elaboration and electrical characterization of Langmuir-Blodgett films of 4-mercaptoaniline functionalized platinum nanoparticles. Chem. Mater. **13**, 1512–1517 (2001)
46. M. Sastry, M. Rao, K.N. Ganesh, Electrostatic assembly of nanoparticles and biomacromolecules. Acc. Chem. Res. **35**, 847–855 (2002)

47. S. Datta, J. Biswas, S. Bhattacharya, How does spacer length of imidazolium gemini surfactants control the fabrication of 2D-Langmuir films of silver-nanoparticles at the air-water interface. J. Colloid Interface Sci. **430**, 85–92 (2014)
48. V. Sashuk, R. Holyst, T. Wojciechowski, M. Fialkowski, Close-packed monolayers of charged Janus-type nanoparticles at the air-water interface. J. Colloid Interface Sci. **375**, 180–186 (2012)
49. M. Benkovicova, K. Vegsoe, P. Siffalovic, M. Jergel, E. Majkova, S. Luby, A. Satka, Preparation of sterically stabilized gold nanoparticles for plasmonic applications. Chem. Pap. **67**, 1225–1230 (2013)
50. Y. Zhang, M.E. Grass, S.E. Habas, F. Tao, T. Zhang, P. Yang, G.A. Somorjai, One-step polyol synthesis and langmuir-blodgett monolayer formation of size-tunable monodisperse rhodium nanocrystals with catalytically active (111) surface structures. J. Phys. Chem. C **111**, 12243–12253 (2007)
51. K.L. Genson, J. Holzmueller, C. Jiang, J. Xu, J.D. Gibson, E.R. Zubarev, V.V. Tsukruk, Langmuir-Blodgett monolayers of gold nanoparticles with amphiphilic shells from V-shaped binary polymer arms. Langmuir **22**, 7011–7015 (2006)
52. A. Tao, P. Sinsermsuksakul, P. Yang, Tunable plasmonic lattices of silver nanocrystals. Nat. Nanotechnol. **2**, 435–440 (2007)
53. E. Bellido, N. Domingo, I. Ojea-Jimenez, D. Ruiz-Molina, Structuration and integration of magnetic nanoparticles on surfaces and devices. Small **8**, 1465–1491 (2012)
54. Y. Wang, M. Yang, B. Xu, Z. Yang, N. Hu, L. Wei, B. Cai, Y. Zhang, Controlled assembly of FePt nanoparticles monolayer on solid substrates. J. Colloid Interface Sci. **417**, 100–108 (2014)
55. M. Wen, E. Kejia, H. Qi, L. Li, J. Chen, Y. Chen, Q. Wu, T. Zhang, Langmuir-Blodgett self-assembly and electrochemical catalytic property of FePt magnetic nano-monolayer. J. Nanopart. Res. **9**, 909–917 (2007)
56. M. Kumar, A. Pathak, M. Singh, M.L. Singla, Fabrication of Langmuir-Blodgett film from polyvinylpyrrolidone stabilized NiCo alloy nanoparticles. Thin Solid Films **519**, 1445–1451 (2010)
57. S. Kundu, Layer-by-layer assembly of thiol-capped Au nanoparticles on a water surface and their deposition on H-terminated Si(001) by the Langmuir-Blodgett method. Langmuir **27**, 3930–3936 (2011)
58. S. Kundu, J.K. Bal, Reorganization of Au nanoparticle Langmuir-Blodgett films on wet chemically passivated Si(001) surfaces. J. Appl. Phys. **110** (2011)
59. S. Kundu, K. Das, O. Konovalov, Prolonged reorganization of thiol-capped Au nanoparticles layered structures. AIP Adv. **3** (2013)
60. M.M. de Villiers, D.P. Otto, S.J. Strydom, Y.M. Lvov, Introduction to nanocoatings produced by layer-by-layer (LbL) self-assembly. Adv. Drug Delivery Rev. **63**, 701–715 (2011)
61. G. Decher, J.B. Schlenoff (eds.), *Multilayer Thin Films: Sequential Assembly of Nanocomposite Materials* (Wiley-VCH Verlag GmbH & Co. KGaA, 2012)
62. A.N. Shipway, E. Katz, I. Willner, Nanoparticle arrays on surfaces for electronic, optical, and sensor applications. ChemPhysChem **1**, 18–52 (2000)
63. A.N. Shipway, I. Willner, Nanoparticles as structural and functional units in surface-confined architectures. Chem. Commun. **20**, 2035–2045 (2001)
64. R.K. Iler, Multilayers of colloidal particles. J. Colloid Interface Sci. **21**, 569–575 (1966)
65. J.R. Siqueira Jr, L. Caseli, F.N. Crespilho, V. Zucolotto, O.N. Oliveira Jr, Immobilization of biomolecules on nanostructured films for biosensing. Biosens. Bioelectron. **25**, 1254–1263 (2010)
66. K. Sato, J. Anzai, Dendrimers in layer-by-layer assemblies: synthesis and applications. Molecules **18**, 8440–8460 (2013)
67. J. Schmitt, G. Decher, W.J. Dressick, S.L. Brandow, R.E. Geer, R. Shashidhar, J.M. Calvert, Metal nanoparticle/polymer superlattice films: fabrication and control of layer structure. Adv. Mater. **9**, 61–65 (1997)

68. A.I. Abdelrahman, A.M. Mohammad, T. Okajima, T. Ohsaka, Fabrication and electrochemical application of three-dimensional gold nanoparticles: self-assembly. J. Phys. Chem. B **110**, 2798–2803 (2006)
69. A.I. Abdelrahman, A.M. Mohammad, M.S. El-Deab, T. Okajima, T. Ohsaka, Bisthiol-assisted multilayers' self-assembly of gold nanoparticles: synthesis, characterization, size control and electrocatalytic applications. Macromol. Symp. **270**, 74–81 (2008)
70. J.F. Hicks, Y. Seok-Shon, R.W. Murray, Layer-by-layer growth of polymer/nanoparticle films containing monolayer-protected gold clusters. Langmuir **18**, 2288–2294 (2002)
71. W. Song, M. Okamura, T. Kondo, K. Uosaki, Sequential layer-by-layer growth of Au nanoclusters protected by a mixed self-assembled monolayer with a polymer binding layer—effects of pH and ionic strength of the polymer solution. J. Electroanal. Chem. **612**, 105–111 (2008)
72. W.B. Zhao, J. Park, A.-M. Caminade, S.-J. Jeong, Y.H. Jang, S.O. Kim, J.-P. Majoral, J. Cho, D.H. Kim, Localized surface plasmon resonance coupling in Au nanoparticles/phosphorus dendrimer multilayer thin films fabricated by layer-by-layer self-assembly method. J. Mater. Chem. **19**, 2006–2012 (2009)
73. B. Peter, S. Kurunczi, D. Patko, I. Lagzi, B. Kowalczyk, Z. Rácz, B.A. Grzybowski, R. Horvath, Label-free in situ optical monitoring of the adsorption of oppositely charged metal nanoparticles. Langmuir **30**, 13478–13482 (2014)
74. S. Kawada, D. Saeki, H. Matsuyama, Development of ultrafiltration membrane by stacking of silver nanoparticles stabilized with oppositely charged polyelectrolytes. Colloids Surf. A **451**, 33–37 (2014)
75. Y. Liu, Y. Wang, R.O. Claus, Layer-by-layer ionic self-assembly of Au colloids into multilayer thin-films with bulk metal conductivity. Chem. Phys. Lett. **298**, 315–319 (1998)
76. P.J. Rivero, J. Goicoechea, I.R. Matias, F.J. Arregui, A comparative study of two different approaches for the incorporation of silver nanoparticles into layer-by-layer films. Nanoscale Res. Lett. **9**, 301–301 (2014)
77. Y. Ko, H. Baek, Y. Kim, M. Yoon, J. Cho, Hydrophobic nanoparticle-based nanocomposite films using in situ ligand exchange layer-by-layer assembly and their nonvolatile memory applications. ACS Nano **7**, 143–153 (2012)
78. M. Park, Y. Kim, Y. Ko, S. Cheong, S.W. Ryu, J. Cho, Amphiphilic layer-by-layer assembly overcoming solvent polarity between aqueous and nonpolar media. J. Am. Chem. Soc. **136**, 17213–17223 (2014)
79. N. Krasteva, I. Besnard, B. Guse, R.E. Bauer, K. Müllen, A. Yasuda, T. Vossmeyer, Self-assembled gold nanoparticle/dendrimer composite films for vapor sensing applications. Nano Lett. **2**, 551–555 (2002)
80. M.D. Musick, C.D. Keating, M.H. Keefe, M.J. Natan, Stepwise construction of conductive Au colloid multilayers from solution. Chem. Mater. **9**, 1499–1501 (1997)
81. M.D. Musick, C.D. Keating, L.A. Lyon, S.L. Botsko, D.J. Pena, W.D. Holliway, T.M. McEvoy, J.N. Richardson, M.J. Natan, Metal films prepared by stepwise assembly. 2. Construction and characterization of colloidal Au and Ag multilayers. Chem. Mater. **12**, 2869–2881 (2000)
82. T. Baum, D. Bethell, M. Brust, D.J. Schiffrin, Electrochemical charge injection into immobilized nanosized gold particle ensembles: potential modulated transmission and reflectance spectroscopy. Langmuir **15**, 866–871 (1999)
83. M. Brust, R. Etchenique, E.J. Calvo, G.J. Gordillo, The self-assembly of gold and SCd nanoparticle multilayer structures studied by quartz crystal microgravimetry. Chem. Commun. 1949–1950 (1996)
84. L. Supriya, R.O. Claus, Colloidal Au/linker molecule multilayer films: low-temperature thermal coalescence and resistance changes. Chem. Mater. **17**, 4325–4334 (2005)
85. J. Dhar, S. Patil, Self-assembly and catalytic activity of metal nanoparticles immobilized in polymer membrane prepared via layer-by-layer approach. ACS Appl. Mater. Interfaces **4**, 1803–1812 (2012)

86. H. Li, Z. Li, L. Wu, Y. Zhang, M. Yu, L. Wei, Constructing metal nanoparticle multilayers with polyphenylene dendrimer/gold nanoparticles via "click" chemistry. Langmuir **29**, 3943–3949 (2013)
87. J.W. Goodby, P.J. Collings, T. Kato, C. Tschierske, H. Gleeson, P. Raynes (eds.), *Handbook of Liquid Crystals* (Wiley-VCH Verlag & Co. KGaA, 2013)
88. M. Sawamura, K. Kawai, Y. Matsuo, K. Kanie, T. Kato, E. Nakamura, Stacking of conical molecules with a fullerene apex into polar columns in crystals and liquid crystals. Nature **419**, 702–705 (2002)
89. B. Donnio, S. Buathong, I. Bury, D. Guillon, Liquid crystalline dendrimers. Chem. Soc. Rev. **36**, 1495–1513 (2007)
90. G.L. Nealon, R. Greget, C. Dominguez, Z.T. Nagy, D. Guillon, J.-L. Gallani, B. Donnio, Liquid-crystalline nanoparticles: hybrid design and mesophase structures. Beilstein J. Org. Chem. **8**, 349–370 (2012)
91. H.K. Bisoyi, S. Kumar, Liquid-crystal nanoscience: an emerging avenue of soft self-assembly. Chem. Soc. Rev. **40**, 306–319 (2011)
92. J. van Herrikhuyzen, G. Portale, J.C. Gielen, P.C.M. Christianen, N.A.J.M. Sommerdijk, S. C.J. Meskers, A.P.H.J. Schenning, Disk micelles from amphiphilic Janus gold nanoparticles. Chem. Commun. 697–699 (2008)
93. P. Davidson, J.C.P. Gabriel, Mineral liquid crystals. Curr. Opin. Colloid Interface Sci. **9**, 377–383 (2005)
94. U. Shivakumar, J. Mirzaei, X. Feng, A. Sharma, P. Moreira, T. Hegmann, Nanoparticles: complex and multifaceted additives for liquid crystals. Liq. Cryst. **38**, 1495–1514 (2011)
95. T. Hegmann, Modulating the properties of liquid crystals using nanoparticles as dopants. Int. Innov. Rep. **9**, 53–55 (2013)
96. M.C. Daniel, D. Astruc, Gold nanoparticles: assembly, supramolecular chemistry, quantum-size-related properties, and applications toward biology, catalysis, and nanotechnology. Chem. Rev. **104**, 293–346 (2004)
97. M. Brust, M. Walker, D. Bethell, D.J. Schiffrin, R. Whyman, Synthesis of thiol-derivatised gold nanoparticles in a two-phase Liquid-Liquid system. J. Chem. Soc., Chem. Commun. 801–802 (1994)
98. P.J.G. Goulet, R.B. Lennox, New insights into Brust–Schiffrin metal nanoparticle synthesis. J. Am. Chem. Soc. **132**, 9582–9584 (2010)
99. N.R. Jana, X. Peng, Single-phase and gram-scale routes toward nearly monodisperse Au and other noble metal nanocrystals. J. Am. Chem. Soc. **125**, 14280–14281 (2003)
100. X. Mang, X. Zeng, B. Tang, F. Liu, G. Ungar, R. Zhang, L. Cseh, G.H. Mehl, Control of anisotropic self-assembly of gold nanoparticles coated with mesogens. J. Mater. Chem. **22**, 11101–11106 (2012)
101. X. Ji, D. Copenhaver, C. Sichmeller, X. Peng, Ligand bonding and dynamics on colloidal nanocrystals at room temperature: the case of alkylamines on CdSe nanocrystals. J. Am. Chem. Soc. **130**, 5726–5735 (2008)
102. R.C. Hedden, B.J. Bauer, A.P. Smith, F. Gröhn, E. Amis, Templating of inorganic nanoparticles by PAMAM/PEG dendrimer–star polymers. Polymer **43**, 5473–5481 (2002)
103. W. Jia, J. McLachlan, J. Xu, S.M. Tadayyon, P.R. Norton, S.H. Eichhorn, Characterization of Au and Pd nanoparticles by high-temperature TGA–MS. Can. J. Chem. **84**, 998–1005 (2006)
104. M. Iqbal, J. McLachlan, W. Jia, N. Braidy, G. Botton, S.H. Eichhorn, Ligand effects on the size and purity of Pd nanoparticles. J. Therm. Anal. Calorim. **96**, 15–20 (2009)
105. W. Jia, J. McLachlan, J. Xu, S.H. Eichhorn, Size and purity of gold nanoparticles changes with different types of thiolate ligands. J. Therm. Anal. Calorim. **100**, 839–845 (2010)
106. R. Ristau, R. Tiruvalam, P.L. Clasen, E.P. Gorskowski, M.P. Harmer, C.J. Kiely, I. Hussain, M. Brust, Electron microscopy studies of the thermal stability of gold nanoparticle arrays. Gold Bull. **42**, 133–143 (2009)

107. Y. Joseph, I. Besnard, M. Rosenberger, B. Guse, H.-G. Nothofer, J.M. Wessels, U. Wild, A. Knop-Gericke, D. Su, R. Schlögl, A. Yasuda, T. Vossmeyer, Self-assembled gold nanoparticle/alkanedithiol films: preparation, electron microscopy, XPS-analysis, charge transport, and vapor-sensing properties. J. Phys. Chem. B **107**, 7406–7413 (2003)
108. M. Draper, I.M. Saez, S.J. Cowling, P. Gai, B. Heinrich, B. Donnio, D. Guillon, J.W. Goodby, Self-assembly and shape morphology of liquid crystalline gold metamaterials. Adv. Funct. Mater. **21**, 1260–1278 (2011)
109. J. Mirzaei, M. Urbanski, H.-S. Kitzerow, T. Hegmann, Synthesis of liquid crystal silane-functionalized gold nanoparticles and their effects on the optical and electro-optic properties of a structurally related nematic liquid crystal. ChemPhysChem **15**, 1381–1394 (2014)
110. N. Kanayama, O. Tsutsumi, A. Kanazawa, T. Ikeda, Distinct thermodynamic behaviour of a mesomorphic gold nanoparticle covered with a liquid-crystalline compound. Chem. Commun. 2640–2641 (2001)
111. B. Donnio, Liquid-crystalline metallodendrimers. Inorg. Chim. Acta **409**, 53–67 (2014)
112. I. In, Y.-W. Jun, Y.J. Kim, S.Y. Kim, Spontaneous one dimensional arrangement of spherical Au nanoparticles with liquid crystal ligands. Chem. Commun. 800–801 (2005)
113. S. Frein, J. Boudon, M. Vonlanthen, T. Scharf, J. Barbera, G. Suess-Fink, T. Buergi, R. Deschenaux, Liquid-crystalline thiol- and disulfide-based dendrimers for the functionalization of gold nanoparticles. Helv. Chim. Acta **91**, 2321–2337 (2008)
114. X. Zeng, F. Liu, A.G. Fowler, G. Ungar, L. Cseh, G.H. Mehl, J.E. Macdonald, 3D ordered gold strings by coating nanoparticles with mesogens. Adv. Mater. **21**, 1746–1750 (2009)
115. L. Cseh, G.H. Mehl, The design and investigation of room temperature thermotropic nematic gold nanoparticles. J. Am. Chem. Soc. **128**, 13376–13377 (2006)
116. L. Cseh, G.H. Mehl, Structure-property relationships in nematic gold nanoparticles. J. Mater. Chem. **17**, 311–315 (2007)
117. M. Wojcik, W. Lewandowski, J. Matraszek, J. Mieczkowski, J. Borysiuk, D. Pociecha, E. Gorecka, Liquid-crystalline phases made of gold nanoparticles. Angew. Chem. Int. Ed. **48**, 5167–5169 (2009)
118. M. Wojcik, M. Kolpaczynska, D. Pociecha, J. Mieczkowski, E. Gorecka, Multidimensional structures made by gold nanoparticles with shape-adaptive grafting layers. Soft Matter **6**, 5397–5400 (2010)
119. J.M. Wolska, D. Pociecha, J. Mieczkowski, E. Gorecka, Gold nanoparticles with flexible mesogenic grafting layers. Soft Matter **9**, 3005–3008 (2013)
120. K. Kaneko, A. Mandai, B. Heinrich, B. Donnio, T. Hanasaki, Electric-field-induced reversible viscosity change in a columnar liquid crystal. ChemPhysChem **11**, 3596–3598 (2010)
121. V.M. Marx, H. Girgis, P.A. Heiney, T. Hegmann, Bent-core liquid crystal (LC) decorated gold nanoclusters: synthesis, self-assembly, and effects in mixtures with bent-core LC hosts. J. Mater. Chem. **18**, 2983–2994 (2008)
122. B.M. Rosen, C.J. Wilson, D.A. Wilson, M. Peterca, M.R. Imam, V. Percec, Dendron-mediated self-assembly, disassembly, and self-organization of complex systems. Chem. Rev. **109**, 6275–6540 (2009)
123. B. Donnio, P. García-Vázquez, J.L. Gallani, D. Guillon, E. Terazzi, Dendronized ferromagnetic gold nanoparticles self-organized in a termotropic cubic phase. Adv. Mater. **19**, 3534–3539 (2007)
124. K. Kanie, M. Matsubara, X. Zeng, F. Liu, G. Ungar, H. Nakamura, A. Muramatsu, Simple cubic packing of gold nanoparticles through rational design of their dendrimeric corona. J. Am. Chem. Soc. **134**, 808–811 (2012)
125. A. Demortiere, S. Buathong, B.P. Pichon, P. Panissod, D. Guillon, S. Begin-Colin, B. Donnio, Nematic-like organization of magnetic mesogen-hybridized nanoparticles. Small **6**, 1341–1346 (2010)
126. B. Donnio, A. Derory, E. Terazzi, M. Drillon, D. Guillon, J.-L. Gallani, Very slow high-temperature relaxation of the remnant magnetic moment in 2 nm mesomorphic gold nanoparticles. Soft Matter **6**, 965–970 (2010)

127. A. Demortiere, P. Panissod, B.P. Pichon, G. Pourroy, D. Guillon, B. Donnio, S. Begin-Colin, Size-dependent properties of magnetic iron oxide nanocrystals. Nanoscale **3**, 225–232 (2011)
128. S. Kumar, S.K. Pal, P.S. Kumar, V. Lakshminarayanan, Novel conducting nanocomposites: synthesis of triphenylene-covered gold nanoparticles and their insertion into a columnar matrix. Soft Matter **3**, 896–900 (2007)
129. Z. Shen, M. Yamada, M. Miyake, Control of stripelike and hexagonal self-assembly of gold nanoparticles by the tuning of interactions between triphenylene ligands. J. Am. Chem. Soc. **129**, 14271–14280 (2007)
130. W. Lewandowski, D. Constantin, K. Walicka, D. Pociecha, J. Mieczkowski, E. Gorecka, Smectic mesophases of functionalized silver and gold nanoparticles with anisotropic plasmonic properties. Chem. Commun. **49**, 7845–7847 (2013)